# ALBATROSS - Progress Report for 1st Quarterly Review

For the attention of: Jérôme BENVENISTE – ESA

| | Function | Name | Signature | Date |
|---|---|---|---|---|
| Prepared by | Project manager/<br>Project Team | Mathilde CANCET<br>Ole ANDERSEN<br>Florent LYARD<br>Geir MOHOLDT<br>Michel TSAMADOS | | 09/03/22 |
| Approved by | Deputy CEO | Mahmoud EL HAJJ | | 09/03/22 |
| Accepted by | | Date: 2022.03.12<br>'22:57:28 +01'00 | Digitally signed by<br>Jérôme Benveniste | |

153 rue du Lac – 31670 Labège – France
Tél. : +33 (0)562 88 11 11 – Fax : +33 (0)562 88 11 12 – E-mail : noveltis@noveltis.fr

© NOVELTIS, DTU, UCL, NPI 2021
This document is the property of NOVELTIS, no part of it shall be reproduced or transmitted without the express prior written authorisation of NOVELTIS

# Distribution list

| INTERNAL | EXTERNAL | |
|---|---|---|
| **Name** | **Name** | **Company / Organisation** |
| Documentation NOVELTIS<br>Richard BRU<br>Project Team | Jérôme BENVENISTE<br>Marco RESTANO | ESA<br>SERCO/ESA |

© NOVELTIS, DTU, UCL, NPI 2021
This document is the property of NOVELTIS, no part of it shall be reproduced or transmitted without the express prior written authorisation of NOVELTIS

# Document status

| ALBATROSS - Progress Report for 1st Quarterly Review | | | |
|---|---|---|---|
| **Issue** | **Revision** | **Date** | **Reason for the revision** |
| 1 | 0 | 26/11/2021 | Initial version |
| 1 | 1 | 03/03/2022 | Edits following ESA's review |
| 1 | 2 | 09/03/2022 | Minor edits following ESA's comments |

| **Modification status** | | | | |
|---|---|---|---|---|
| Issue | Rev | Status * | Modified pages | Reason for the modification |
| 1 | 1 | M | §2.1, §2.2, §3.2, §3.3, §3.4 | Edits following ESA's review of the initial version. |
| 1 | 2 | M | §2.2 | Minor edits following ESA's comments. |
| | | | | |
| | | | | |
| | | | | |
| | | | | |
| | | | | |
| | | | | |
| | | | | |
| | | | | |
| | | | | |

* *I = Inserted* *D = Deleted* *M = Modified*

© NOVELTIS, DTU, UCL, NPI 2021
This document is the property of NOVELTIS, no part of it shall be reproduced or transmitted without the express prior written authorisation of NOVELTIS

# Acronyms

| | |
|---|---|
| ALBATROSS | ALtimetry for BAthymetry and Tide Retrievals for the Southern Ocean, Sea ice and ice Shelves |
| ATM | Airborne Topographic Mapper |
| DTU | Danish Technical University |
| EIGEN | European Improved Gravity field of the Earth by New techniques |
| ENVISAT | ENVIronment SATellite |
| ERS | European Remote-Sensing satellite |
| ESA | European Space Agency |
| FES | Finite Element Solution |
| GEBCO | General Bathymetric Chart of the Oceans |
| GPS | Global Positioning System |
| GSHHS | Global Self-consistent, Hierarchical, High-resolution Shoreline |
| IBCSO | International Bathymetric Chart of the Southern Ocean |
| LEGOS | Laboratoire d'Etudes en Géophysique et Océanographie Spatiale (laboratory) |
| LIENSs | LIttoral ENvironnement et Sociétés (laboratory) |
| MISR | Multi-angle Imaging SpectroRadiometer |
| MODIS | Moderate-Resolution Imaging Spectroradiometer |
| NASA | National Aeronautics and Space Administration |
| NPI | Norwegian Polar Institute |
| OIB | Operation Ice Bridge |
| OBSPM | Observatoire de Paris-Meudon |
| PDF | Probability Density Function |
| REMA | Reference Elevation Model of Antarctica |
| SAMOSA | SAR Altimetry MOde Studies and Applications |
| SAR | Synthetic-Aperture Radar |
| SMOS | Soil Moisture and Ocean Salinity |
| TUGO | Toulouse Unstructured Grid Ocean model |
| UCL | University College London |

© NOVELTIS, DTU, UCL, NPI 2021
This document is the property of NOVELTIS, no part of it shall be reproduced or transmitted without the express prior written authorisation of NOVELTIS

# References

Abulaitijiang, A., Andersen, O. B., Sandwell, D. (2019) Improved Arctic Ocean Bathymetry Derived from DTU17 Gravity Model, Earth and Space Science, vol: 6, issue: 8, pages: 1336-1347, DOI: https://doi.org/10.1029/2018EA000502

Andersen, O.B., Zhang, S., Sandwell, D.T. Smith, W.H.F., Abulaitijiang, A. (2021), The unique role of the Jason geodetic missions for high resolution gravity field and mean sea surface modelling, Remote Sensing, 2021, 13(4), pp. 1–11, 646.

Andersen, O. B., 1995: Global ocean tides from ERS-1 and TOPEX/Poseidon. J. Geophys. Res., 100, 25249–25259. https://doi.org/10.1029/95JC01389

Andersen O. B, Knudsen P (2009) The DNSC08 mean sea surface and mean dynamic topography. J. Geophys. Res., 114, C11, doi:10.1029/2008JC005179, 2009.

Arndt, J. E., Schenke, H. W., Jakobsson, M., Nitsche, F.-O., Buys, G., Goleby, B., Rebesco, M., Bohoyo, F., Hong, J. K., Black, J., Greku, R. K., Udintsev, G. B., Barrios, F., Reynoso-Peralta, W., Taisei, M., Wigley, R. (2013): The International Bathymetric Chart of the Southern Ocean (IBCSO) - digital bathymetric model. PANGAEA, https://doi.org/10.1594/PANGAEA.805734, In supplement to: Arndt, JE et al. (2013): The International Bathymetric Chart of the Southern Ocean Version 1.0 – A new bathymetric compilation covering circum-Antarctic waters. Geophysical Research Letters, 40(9), 1-7, https://doi.org/10.1002/grl.50413

Cancet, M., Andersen, O.B., Lyard, F., Cotton, D., Benveniste, J. (2018), Arctide2017, A High Resolution Regional Tidal Model in the Arctic Ocean, Advances in Space Research, 62(6), 1324-1343, doi: https://doi.org/10.1016/j.asr.2018.01.007

Carrère L., Lyard F., Cancet M., Sahuc E., Allain D., Faugère Y., Dibarboure G., Picot N. (2020), A new global ocean barotropic tide model: FES2022. Presentation at the OSTST virtual meeting in October 2020.

Eisermann, H., Eagles, G., Ruppel, A., Smith, E. C., Jokat, W., & Resources, N. (2020). Bathymetry beneath ice shelves of western Dronning Maud Land, East Antarctica, and implications on ice shelf stability. Geophysical Research Letters, 47.

Foerste, C.; Bruinsma, S.L.; Abrikosov, O-; Lemoine, J-M.; Marty, J.C.; Flechtner, F.; Balmino, G.; Barthelmes, F.; Biancale, R. (2014): EIGEN-6C4, the latest combined global gravity field model including GOCE data up to degree and order 2190 of GFZ Potsdam and GRGS Toulouse. GFZ Data Services. https://doi.org/10.5880/icgem.2015.1

Gardner A. S., Moholdt G., and 5 others. 2018. Increased West Antarctic and unchanged East Antarctic ice discharge over the last 7 years. The Cryosphere, 12, 2, 521-547

Hannah, Charles G., Frédéric Dupont, and Michael Dunphy. Polynyas and tidal currents in the Canadian Arctic Archipelago. Arctic (2009): 83-95.

Howard, S. L., King, M., & Padman, L. (2020) "Antarctic Tide Gauge Database, version 1" U.S. Antarctic Program (USAP) Data Center. doi: https://doi.org/10.15784/601358.

Howat, I. M., Porter, C., Smith, B. E., Noh, M.-J., and Morin, P.: The Reference Elevation Model of Antarctica, The Cryosphere, 13, 665-674, https://doi.org/10.5194/tc-13-665-2019, 2019.

Jena, B., M. Ravichandran, and J. Turner. Recent reoccurrence of large open-ocean polynya on the Maud Rise seamount. Geophysical Research Letters 46.8 (2019): 4320-4329.

Johnson, T., Tsamados, M., Muller, J.-P., and Stroeve, J.: Mapping Arctic Sea Ice Surface Roughness with Multi-angle Imaging SpectroRadiometry, EGU General Assembly 2021, online, 19–30 Apr 2021, EGU21-15897, https://doi.org/10.5194/egusphere-egu21-15897, 2021.

Johnson, T., Tsamados, M. et al (2022), in preparation

© NOVELTIS, DTU, UCL, NPI 2021
This document is the property of NOVELTIS, no part of it shall be reproduced or transmitted without the express prior written authorisation of NOVELTIS

Kurtz, N. T., S. L. Farrell, M. Studinger, N. Galin, J. P. Harbeck, R. Lindsay, V. D. Onana, B. Panzer, and J. G. Sonntag. "Sea ice thickness, freeboard, and snow depth products from Operation IceBridge airborne data." The Cryosphere 7, no. 4 (2013): 1035-1056.

Ligtenberg, S. R. M., M. M. Helsen, and M. R. van den Broeke (2011), An improved semi-empirical model for the densification of Antarctic firn, Cryosphere, 5, 809-819, doi:10.5194/tc-5-809-2011.

Lyard, F. H., Allain, D. J., Cancet, M., Carrère, L., and Picot, N. (2021), FES2014 global ocean tide atlas: design and performance, Ocean Sci., 2021, 17, 615–649, https://doi.org/10.5194/os-17-615-2021

Lythe M. B., Vaughan D. G., and the BEDMAP Consortium (2001), BEDMAP: A new ice thickness and subglacial topographic model of Antarctica, Journal of Geophysical Research, 106, 11335-11351

Matsuoka et al. (2015) Antarctic ice rises and rumples: Their properties and significance for ice-sheet dynamics and evolution. Earth-Science Reviews 150, 724–745.

Mei, M. Jeffrey, and Ted Maksym. "A Textural Approach to Improving Snow Depth Estimates in the Weddell Sea." Remote Sensing 12, no. 9 (2020): 1494.

Morlighem, M., E. Rignot, T. Binder, D. D. Blankenship, R. Drews, G. Eagles, O. Eisen, F. Ferraccioli, R. Forsberg, P. Fretwell, V. Goel, J. S. Greenbaum, H. Gudmundsson, J. Guo, V. Helm, C. Hofstede, I. Howat, A. Humbert, W. Jokat, N. B. Karlsson, W. Lee, K. Matsuoka, R. Millan, J. Mouginot, J. Paden, F. Pattyn, J. L. Roberts, S. Rosier, A. Ruppel, H. Seroussi, E. C. Smith, D. Steinhage, B. Sun, M. R. van den Broeke, T. van Ommen, M. van Wessem, and D. A. Young. 2020. Deep glacial troughs and stabilizing ridges unveiled beneath the margins of the Antarctic ice sheet, Nature Geoscience. 13. 132-137. https://doi.org/10.1038/s41561-019-0510-8

Morlighem, M. 2020. MEaSUREs BedMachine Antarctica, Version 2. Boulder, Colorado USA. NASA National Snow and Ice Data Center Distributed Active Archive Center. doi: https://doi.org/10.5067/E1QL9HFQ7A8M. [Accessed 01/09/2021].

Reiser, Fabian, Sascha Willmes, and Günther Heinemann (2020). A new algorithm for daily Sea Ice lead identification in the arctic and antarctic winter from thermal-infrared satellite imagery. Remote Sensing 12.12 (2020): 1957.

Schaffer, J., Timmermann, R., Arndt, J. E., Rosier, S. H. R., Anker, P. G. D., Callard, S. L., Davis, P. E. D., Dorschel, B., Grob, H., Hattermann, T., Hofstede, C. M., Kanzow, T., Kappelsberger, M., Lloyd, J. M., Ó Cofaigh, C., Roberts, D. H. (2019): An update to Greenland and Antarctic ice sheet topography, cavity geometry, and global bathymetry (RTopo-2.0.4). PANGAEA, https://doi.org/10.1594/PANGAEA.905295, Supplement to: Schaffer, J. et al. (2020): Bathymetry constrains ocean heat supply to Greenland's largest glacier tongue. Nature Geoscience, 13(3), 227-231, https://doi.org/10.1038/s41561-019-0529-x

Schaffer, J., Timmermann, R. (2016): Greenland and Antarctic ice sheet topography, cavity geometry, and global bathymetry (RTopo-2), links to NetCDF files. PANGAEA, https://doi.org/10.1594/PANGAEA.856844, Supplement to: Schaffer, J., Timmermann, R., Arndt, J. E., Kristensen, S. S., Mayer, C., Morlighem, M., Steinhage, D. (2016): A global, high-resolution data set of ice sheet topography, cavity geometry, and ocean bathymetry. Earth System Science Data, 8(2), 543-557, https://doi.org/10.5194/essd-8-543-2016

Smith, E. C., Hattermann, T., Kuhn, G., Gaedicke, C., Berger, S., Drews, R., et al. (2020). Detailed seismic bathymetry beneath Ekström Ice Shelf, Antarctica: Implications for glacial history and ice-ocean interaction. Geophysical Research Letters, 47.

Smith, W. H. F., and D. T. Sandwell (1994), Bathymetric prediction from dense satellite altimetry and sparse shipboard bathymetry, J. Geophys. Res., 99(B11), 21803–21824, doi:10.1029/94JB00988.

Timmermann, R., Le Brocq, A. M., Deen, T. J., Domack, E. W., Dutrieux, P., Galton-Fenzi, B., Hellmer, H. H., Humbert, A., Jansen, D., Jenkins, A., Lambrecht, A., Makinson, K., Niederjasper, F., Nitsche, F.-O., Nøst, O. A., Smedsrud, L. H., Smith, W. (2010): Antarctic ice sheet topography, cavity geometry, and global bathymetry (RTopo 1.0.5-beta). PANGAEA, https://doi.org/10.1594/PANGAEA.741917, Supplement to: Timmermann, R et al. (2010): A consistent dataset of Antarctic ice sheet topography, cavity geometry, and global bathymetry. Earth System Science Data, 2(2), 261-273, https://doi.org/10.5194/essd-2-261-2010

© NOVELTIS, DTU, UCL, NPI 2021
This document is the property of NOVELTIS, no part of it shall be reproduced or transmitted without the express prior written authorisation of NOVELTIS

Zaron, E. D. (2018). Ocean and Ice Shelf Tides from CryoSat-2 Altimetry, Journal of Physical Oceanography, 48(4), 975-993, https://doi.org/10.1175/JPO-D-17-0247.1

© NOVELTIS, DTU, UCL, NPI 2021
This document is the property of NOVELTIS, no part of it shall be reproduced or transmitted without the express prior written authorisation of NOVELTIS

# Table of contents

**1. INTRODUCTION .......... 11**

**2. TIDAL MODELLING AND ALTIMETRY DATA PROCESSING .......... 12**

2.1. IMPLEMENTATION OF THE TIDAL MODEL (NOVELTIS) .......... 12
2.2. ALTIMETRY DATA PROCESSING FOR VALIDATION AND ASSIMILATION (DTU) .......... 15

**3. BATHYMETRY IMPROVEMENT IN THE SOUTHERN OCEAN .......... 19**

3.1. ANALYSIS OF EXISTING BATHYMETRY DATASETS (NOVELTIS) .......... 19
*3.1.1. Inventory of the bathymetry datasets .......... 19*
*3.1.2. Identification of the reference bathymetry dataset .......... 24*
3.2. BATHYMETRY IMPROVEMENT IN THE DEEP OCEAN (DTU) .......... 26
3.3. SEA ICE SURFACE CHARACTERISTICS TO IMPROVE BATHYMETRY GRADIENT LOCATION (UCL) .......... 29
3.4. DATA COLLECTION FOR ICE SHELVES (NPI) .......... 32
3.5. INTEGRATION OF THE BATHYMETRY DATASETS (NOVELTIS) .......... 33
*3.5.1. Case of the Filchner-Ronne ice shelf (Weddell Sea) .......... 33*
*3.5.2. Case of the Amery ice shelf (East Antarctica) .......... 37*

**4. CONCLUSIONS .......... 39**

© NOVELTIS, DTU, UCL, NPI 2021
This document is the property of NOVELTIS, no part of it shall be reproduced or transmitted without the express prior written authorisation of NOVELTIS

# 1. Introduction

The knowledge about bathymetry and ocean tides is at the crossroads of many scientific fields, especially in the Polar regions, as it has significant impact on the ocean circulation modelling and the understanding of the coupled dynamical response of the ocean, sea ice and ice shelves system, the quality and accuracy of sea surface height and sea ice parameter estimates from satellite altimetry, or the understanding of ice-shelf dynamics among others. In isolated regions such as the Southern Ocean, where very few in-situ campaigns are possible, satellite observations bring invaluable information, either directly, with the physical parameters that are measured, or indirectly, considering the strong links between particular characteristics of the parameters and the ocean processes.

The ALBATROSS project aims to improve knowledge about bathymetry and ocean tides in the Southern Ocean.

The project has the following objectives:

- Improve the knowledge on bathymetry around Antarctica thanks to decade-long most recently reprocessed CryoSat datasets, information on bathymetry gradient locations through the analysis of sea ice surface roughness characteristics, and the compilation of the best available data in ice-shelf regions.
- Improve the knowledge on ocean tides in the Southern Ocean through the implementation of a high-resolution hydrodynamic model based on the most advanced developments in terms of ocean tide modelling, and data assimilation of observations, including satellite-altimetry derived tidal retrievals from the most recent and relevant satellite altimetry products.
- Improve satellite altimetry retrievals of sea surface heights and sea ice information.
- Improve the retrievals of ice shelves parameters.
- Share information and knowledge with other Polar science initiatives and projects.

This document is the first Technical Progress Report of the project. It describes the work performed during the first six months of the project, in terms of implementation of the tidal model configuration and developments of new processing strategies to improve the bathymetry knowledge in the region.

© NOVELTIS, DTU, UCL, NPI 2021
This document is the property of NOVELTIS, no part of it shall be reproduced or transmitted without the express prior written authorisation of NOVELTIS

# 2. Tidal modelling and altimetry data processing

## 2.1. Implementation of the tidal model (NOVELTIS)

The implementation of the ALBATROSS tidal atlas in the Southern Ocean follows the same methodology as the regional Arctide2017 model implemented in the Arctic Ocean (Cancet et al., 2018) and the FES2014 global model (Lyard et al., 2021). First, we tune the hydrodynamic model to obtain the best possible hydrodynamic tidal simulation in the region of interest. Second, tidal observations derived from satellite altimetry and in-situ time series of height measurements are used to constrain the hydrodynamic solution through data assimilation.

We use the TUGO hydrodynamic model developed at LEGOS. TUGO is a 2-D/3-D unstructured grid model based on the Navier–Stokes equation in the Boussinesq approximation. It can be used either in time stepping, i.e. running a long simulation (e.g. one year) and then performing tidal harmonic analyses on the resulting tidal elevations and velocities, or in the frequency domain, i.e. directly solving the tidal wave equations for each tidal component separately. The second approach is much less time-consuming in terms of computation, but it can only be used with accurate results for the main linear tidal components. In general, the methodology consists in tuning the parameters of the model in the frequency mode, and then run a long time-stepping simulation to enrich the spectrum of the final atlas with non-linear tidal components.

The first step for the implementation of the hydrodynamic tidal solution consists in defining the model domain extent. Several aspects must be considered to ensure the stability of the simulations. In particular, the boundaries of the model domain should be placed in regions where they do not cross bathymetry gradients or tidal energy flux features.

A first version of the ALBATROSS regional model extent was thus defined following this principle, considering the bathymetry features (Figure 1) and the tidal energy fluxes (Figure 2) in the region. On Figure 2 it can be noted that the tidal energy flux structures are very different for the two main tidal components in the region, M2 and K1.

In addition, the regional model extent was designed to cover the Kerguelen Plateau, which is a region of interest for high-resolution tidal modelling, especially to provide accurate tidal information for the satellite altimetry calibration site maintained by LIENSs (University of La Rochelle) and OBSPM in the Kerguelen Islands.

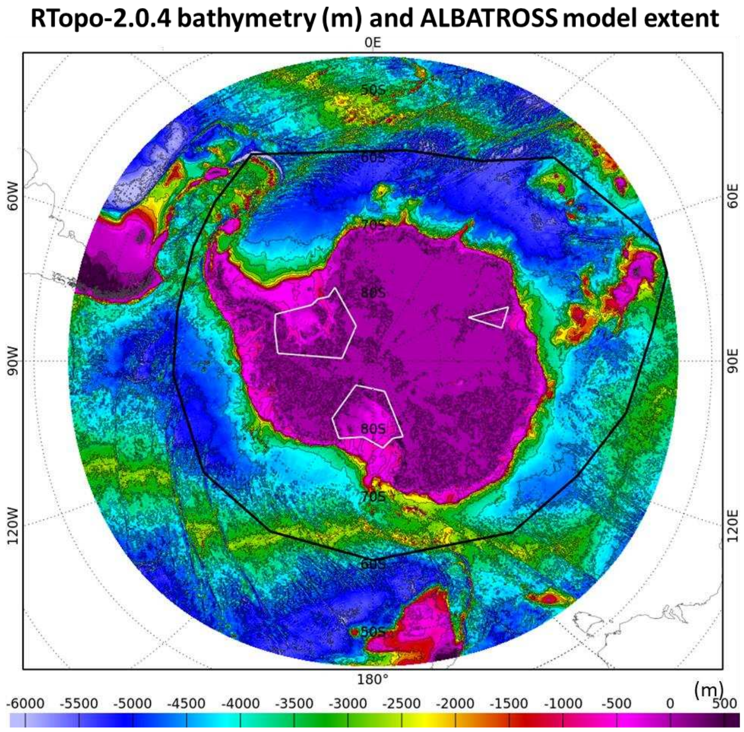


**Figure 1: RTopo-2.0.4 bathymetry (background colour), ALBATROSS model extent version-1 (black polygon) and ice-shelf extents as currently defined in the model (white polygons)**


© NOVELTIS, DTU, UCL, NPI 2021
This document is the property of NOVELTIS, no part of it shall be reproduced or transmitted without the express prior written authorisation of NOVELTIS

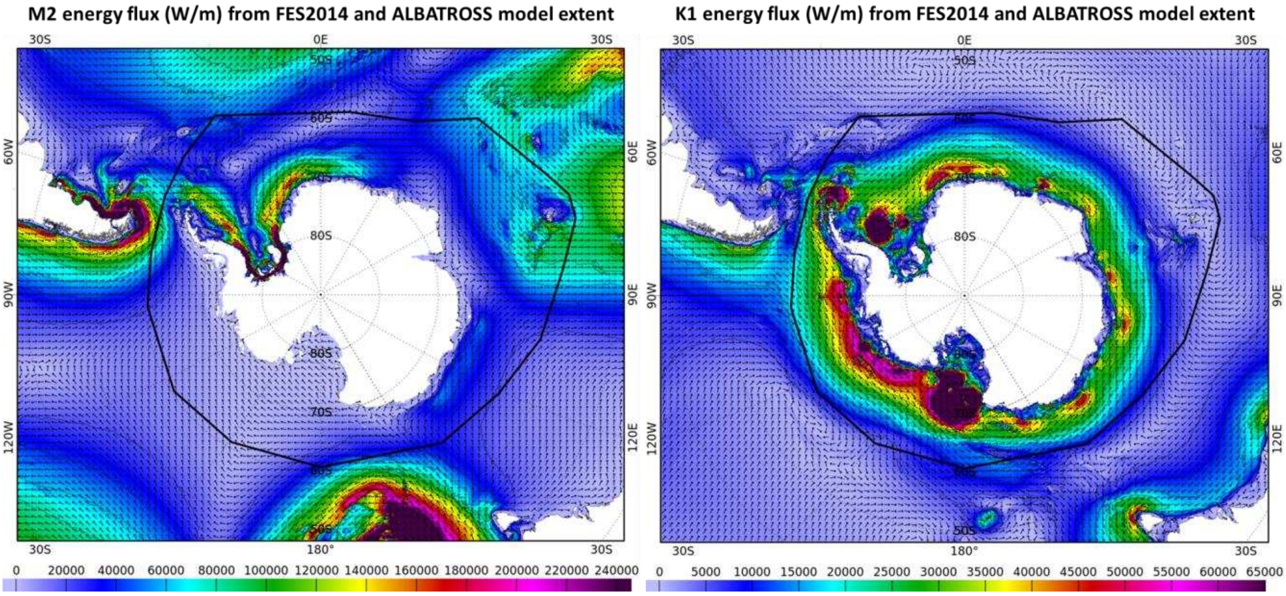


**Figure 2: Tidal energy fluxes (background colour) from the FES2014 global tidal model for the M2 (left) and K1 (right) tidal components, and ALBATROSS model extent version-1 (black polygon)**

A first version of the mesh grid of the regional model was then built within the domain extent, following the GSHHS-2.3.7 coastline. The mesh is an unstructured grid with triangles of various sizes. To define the size of the triangles, several criteria are imposed in the meshing tools, such as the sampling of the coastline, the minimum and maximum resolutions in the deep ocean and on the continental shelves, and the bathymetry gradients.

For the version-1 of the ALBATROSS mesh, criteria close to the under-development FES2022 global model were chosen as a first step, with a maximum resolution of 30 km in the deep ocean and a minimum resolution of 10 km on the continental shelf. Higher resolution (down to 4 km) was imposed in the Weddell Sea and Ross Sea regions. Figure 3 compares the resolution of the mesh grids for the FES2014 global model (a) and the first version of the ALBATROSS regional mesh (b). Within the regional model extent, the number of elements has already been multiplied by a factor 6 from FES2014 to ALBATROSS version-1.

Based on this first version of the regional grid, some sensitivity tests were performed on the parameters of the TUGO hydrodynamic model, mainly the bottom friction and the internal tide wave drag, the latter characterizing the energy transfer from the barotropic mode to the baroclinic mode. The impact of changing the model parameter values is evaluated considering the vector differences with observations, mainly tide gauges and GPS stations located along the Antarctic coastline (database from Howard et al., 2020). Varying the values of the wave drag parameter in the model has a very limited impact on the simulations. On the contrary, there is a clear improvement in the simulations when the friction increases, as the vector differences relative to the tide gauge observations are reduced. The largest variations in the vector differences with the model were observed at some GPS stations located in ice-shelf regions, where the friction with the tides does not only happen at the bottom but also at the interface between the ice and the free water. As the ice friction will be managed separately in the model, these stations were removed from this first evaluation, in order to avoid biasing the bottom friction tuning for the whole model domain with a few ice-shelf stations. This first choice of model parameters will be revisited and refined once the final model grid and the final bathymetry are defined.

All the results of hydrodynamic tidal simulations presented hereinafter in the bathymetry section were obtained with the model configuration based on the mesh grid version-1 and boundary conditions from the FES2014b global model.


© NOVELTIS, DTU, UCL, NPI 2021
This document is the property of NOVELTIS, no part of it shall be reproduced or transmitted without the express prior written authorisation of NOVELTIS

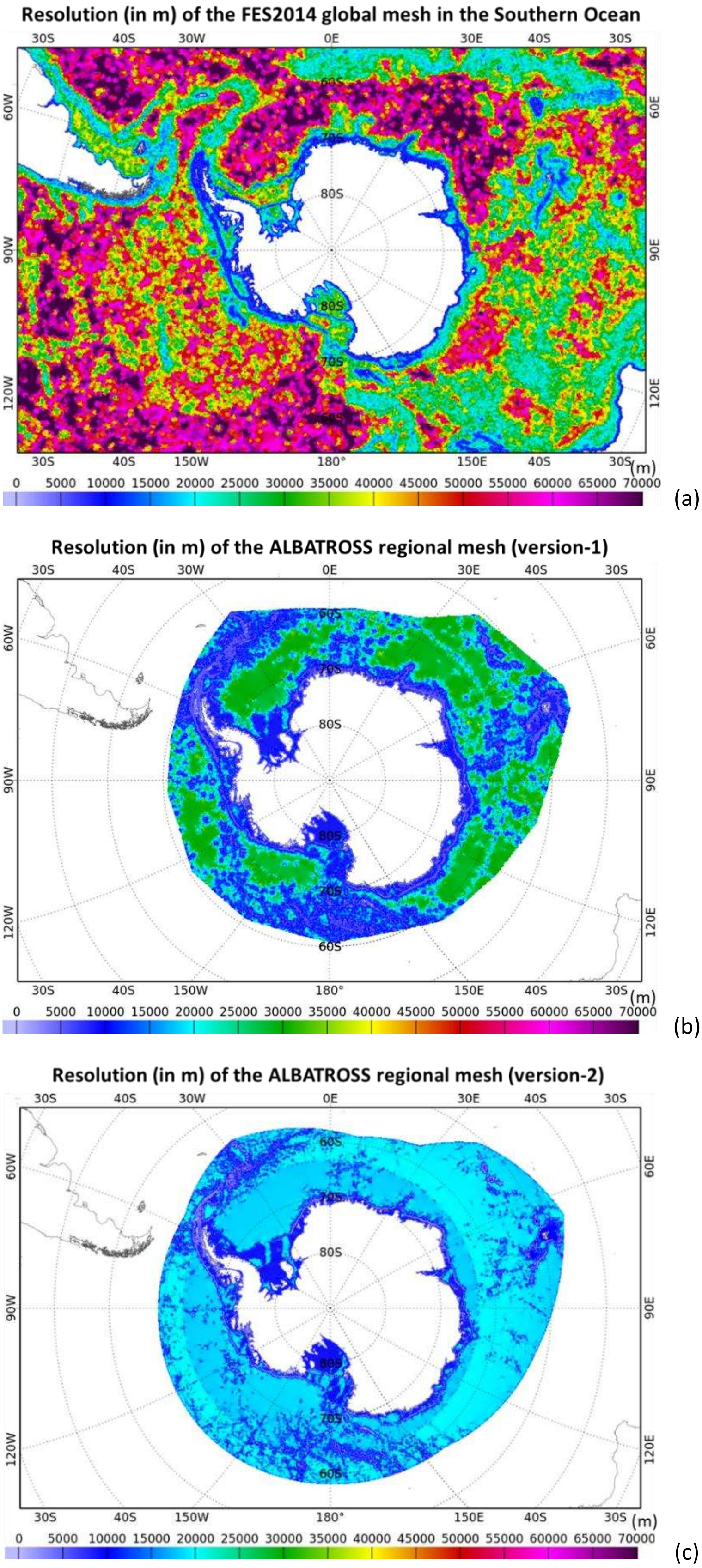


**Figure 3: Resolution of the mesh elements (in meters) of the FES2014 global tidal model (a), the ALBATROSS regional model in version-1 (b) and the ALBATROSS regional model in version-2 (c) in the Southern Ocean.**


© NOVELTIS, DTU, UCL, NPI 2021

This document is the property of NOVELTIS, no part of it shall be reproduced or transmitted without the express prior written authorisation of NOVELTIS

In the meantime, further developments have been made in the meshing tools and in the TUGO model, in order to improve this configuration and the resulting simulations.

Among these new developments, we can mention:

- The possibility to use the loxodromic projection in the meshing tools, resulting in smoother boundaries for the model extent in version-2 (Figure 3, c);
- Some improvements and new strategies in the smoothing of the mesh elements when building the grid, resulting in more homogeneous meshes.

A version-2 of the ALBATROSS mesh grid has been designed using these new developments and is under testing. The resolution has been increased in the deep ocean and on the continental shelf, compared to version-1 (Figure 3, c).

New developments in the TUGO model have also been performed to better take into account the impact of the ice cover in the friction. Up to now, the friction due to the ice cover (sea ice or ice shelf) at the interface with the free ocean water was prescribed as a multiplying factor (generally empirically set to 2) of the bottom friction, in polygons representing the ice cover extent.

In the Southern Ocean, the ice friction was uniformly applied under the ice shelves, in the white polygons shown on Figure 1, with a unique multiplying factor. These new developments enable to prescribe the ice friction with a set of polygons and associated values, with a more flexible control of the regionalized ice-friction settings. This new flexibility in the ice friction prescription will be explored during the ALBATROSS project. The polygons of the ice-shelf extents will be refined, and the sea ice cover will also be considered, as a separate contributor to ice friction.

## 2.2. Altimetry data processing for validation and assimilation (DTU)

A new system for tidal prediction has been developed for the ALBATROSS project. In this system it is possible to use data from various satellites (Jason-suite, Cryosat-2, Saral, ENVISAT, ERS) and to use various combinations of these missions in the prediction of the tides. The argument for this approach is that tidal determination in high latitudes is not straightforward due to frequently questionable alias periods for the tidal constituents.

Consequently, these satellites have various strengths and weaknesses when it comes to different tidal constituents (see Table 1 for CryoSat-2). The well-known problem with sun-synchronous satellites is the ability to estimate sun-synchronous tidal constituents like S2, which maps into the mean.

**Table 1: Alias periods (days) for sample intervals that occur when CryoSat-2 data are accumulated within 30-km spatial bins at 70°S**

| | Sample interval $\Delta t$ (days) | | | | |
|---|---|---|---|---|---|
| | 368.2396 | 28.9410 | 19.4246 | 7.5180 | 1.9983 |
| $M_2$ | 800 | 371 | 42 | 16 | 14 |
| $S_2$ | 768 | 245 | 129 | 209 | 576 |
| $K_2$ | 743 | 715 | 438 | 98 | 267 |
| $N_2$ | 2095 | 225 | 113 | 30 | 9 |
| $K_1$ | 1486 | 1430 | 41 | 16 | 535 |
| $O_1$ | 1262 | 294 | 347 | 638 | 14 |
| $P_1$ | 1591 | 209 | 52 | 15 | 277 |
| $Q_1$ | 5106 | 195 | 55 | 26 | 9 |
| $NO_1$ | 3170 | 962 | 86 | 28 | 29 |
| $MO_3$ | 2187 | 164 | 47 | 16 | 7 |
| $MK_3$ | 1734 | 500 | 1682 | 115 | 15 |
| $M_4$ | 4633 | 185 | 288 | 140 | 7 |

We have processed 9 years of CryoSat-2 data, retracked with the SAMOSA+ physical retracker, through the ESA GPOD SARvatore service for CryoSat-2 (now hosted on the EarthConsole platform, https://earthconsole.eu, as a P-PRO service). Following the approach of Zaron (2018) we investigated the box sizes to accumulate CryoSat-2 data. We found that the main reduction occurs with a box size of 3 degrees in longitude (corresponding to 100 km, also found by Zaron) x 0.5 degrees in latitude. 100 km neatly correspond to sampling CryoSat-2 data within the sub-cycle of 28.941 days. Hence the alias periods in the second column of Table 1 is used for the following investigation. Each CryoSat-2 track

© NOVELTIS, DTU, UCL, NPI 2021
This document is the property of NOVELTIS, no part of it shall be reproduced or transmitted without the express prior written authorisation of NOVELTIS

crossing the chosen box of 0.5 x 3 degrees will be averaged into one averaged observation for the following tidal prediction.

The number of Cryosat-2 observations retracked by SAMOSA+ retracker and processed using the FES2014 ocean tide model are seen in Figure 4. The tidal residuals were estimated using the Tidal response method developed for ESA satellites by Andersen (1995).

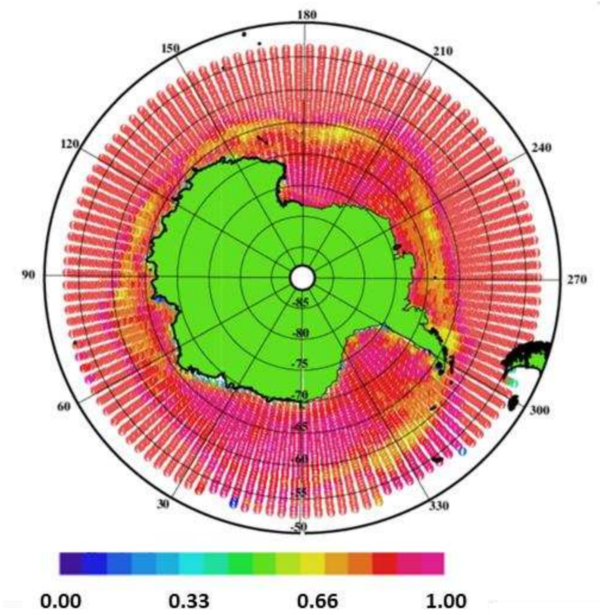


**Figure 4: The number of datapoints used in the estimation of the residual tidal signal within the boxes. The number is given in multiples x 1000.**

In order to demonstrate the importance of the preferable orbit and sampling of CryoSat-2, we performed an estimation of the M2 ocean tide from CryoSat-2 and from repeat observations onboard conventional satellites like Saral/Altika. This is shown in Figure 5. The tidal estimates from conventional satellites like ERS/Envisat/Saral are the data that have been available in former tidal models. Hence it is interesting to observe that the ability to predict tides by Cryosat-2 in the Weddell Sea is providing a fundamentally new dataset for tidal modelling.

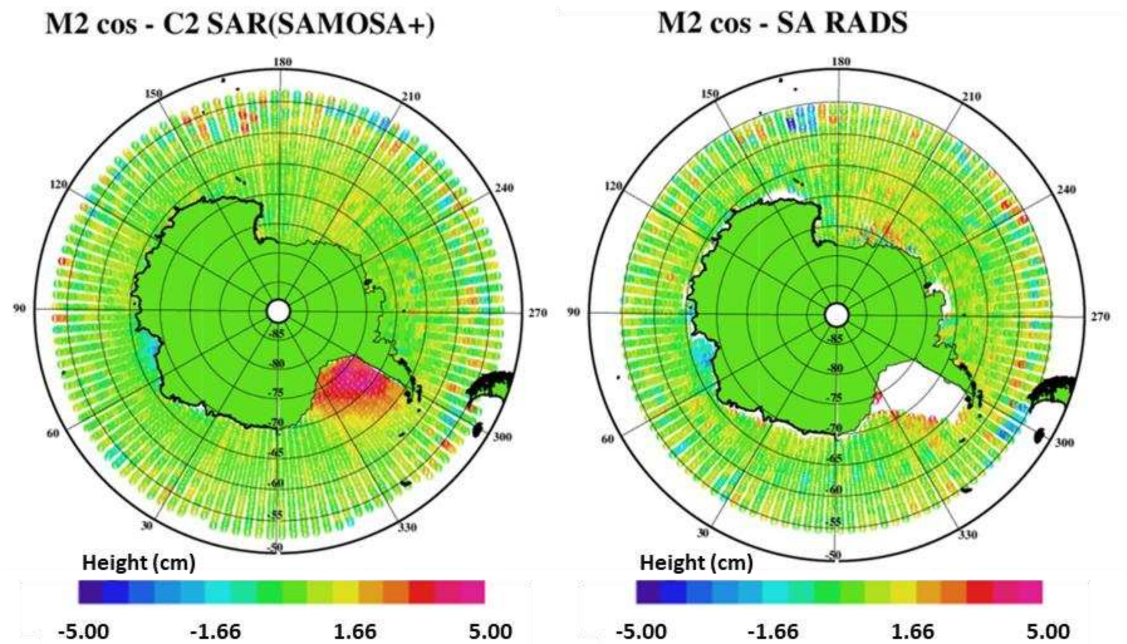


**Figure 5: Comparison of an estimation of the M2 residual constituent from CryoSat-2 (left) and from Saral Altika (right). Notice the strong tidal signal revealed by CryoSat-2 in the Weddell Sea, which has not been seen before from satellite.**

© NOVELTIS, DTU, UCL, NPI 2021
This document is the property of NOVELTIS, no part of it shall be reproduced or transmitted without the express prior written authorisation of NOVELTIS

Figure 6 to Figure 9 show the tidal constituents (cosine and sine) estimated from the CryoSat-2 data for the four main tidal components (M2, S2, K1 and O1). Very coherent tidal structures can be noticed in the Weddell Sea and in the Ross Sea, in particular. Offshore, the tidal estimates contain more noise, which is due to less favourable signal-to-noise ratio, as the tidal amplitudes are much lower.

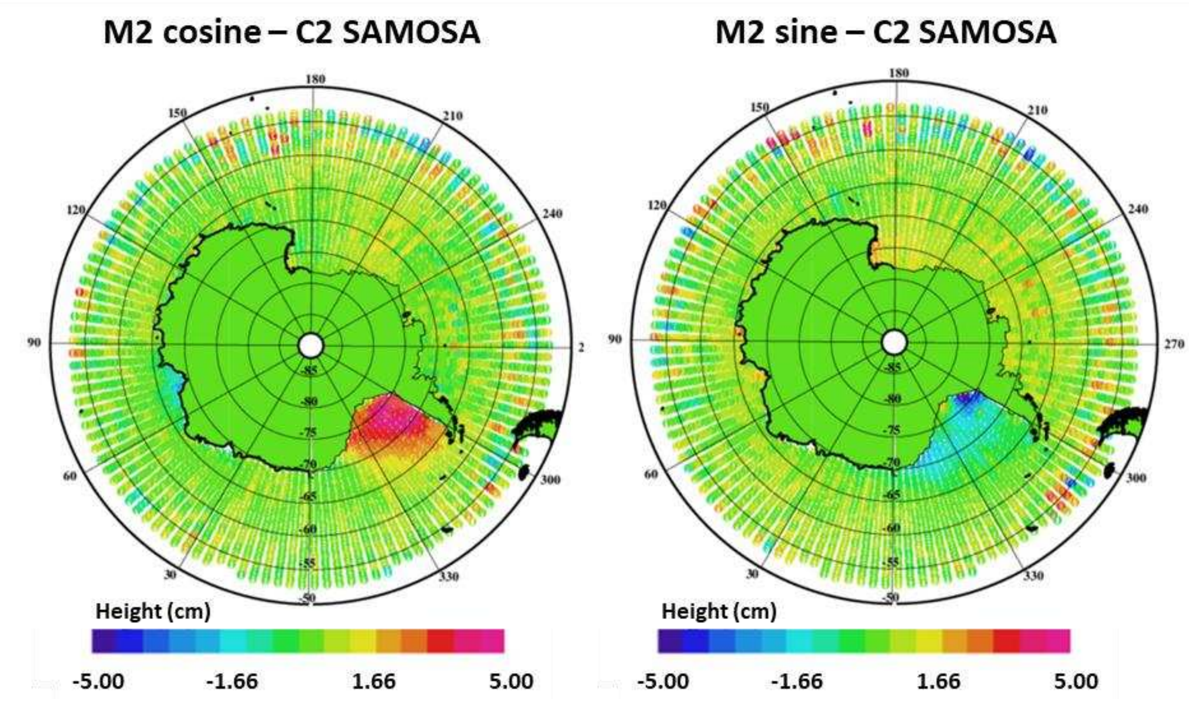


**Figure 6: The cosine and sine components of the M2 tidal residual estimated from CryoSat-2 data.**

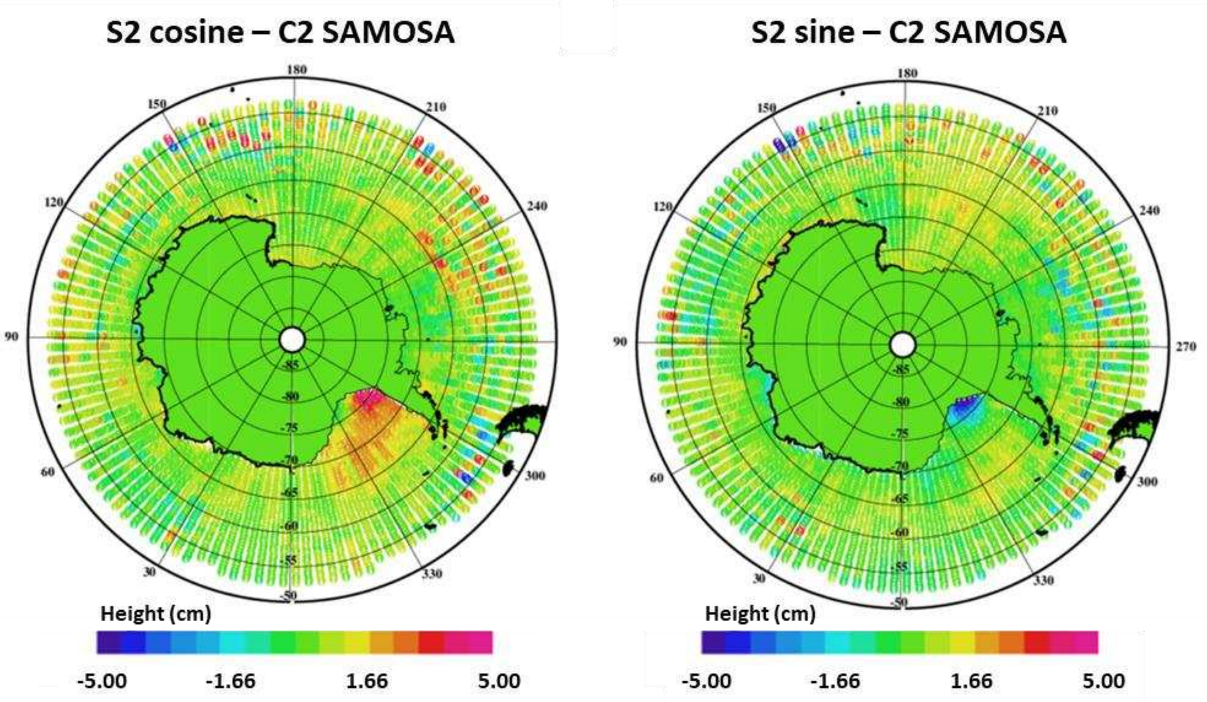


**Figure 7: The cosine and sine components of the S2 tidal residual estimated from CryoSat-2 data.**


© NOVELTIS, DTU, UCL, NPI 2021

This document is the property of NOVELTIS, no part of it shall be reproduced or transmitted without the express prior written authorisation of NOVELTIS

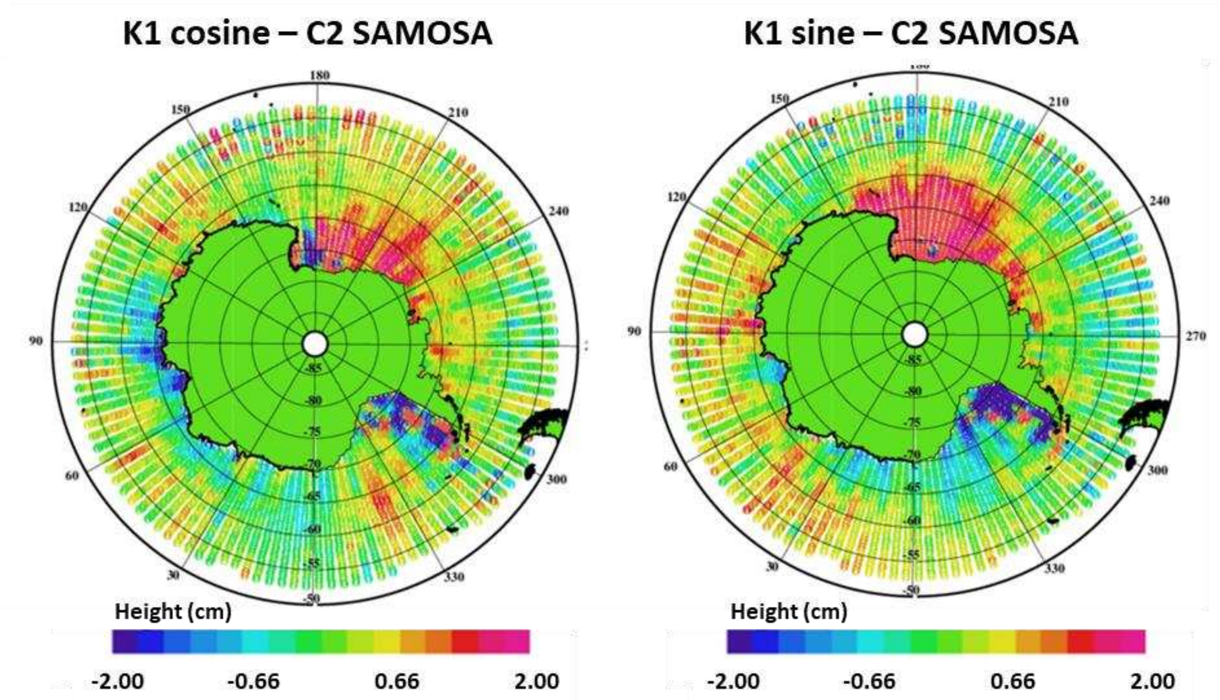


**Figure 8: The cosine and sine components of the K1 tidal residual estimated from CryoSat-2 data. Notice the colour scale is reduced to +/- 2 cm compared with previous plots.**

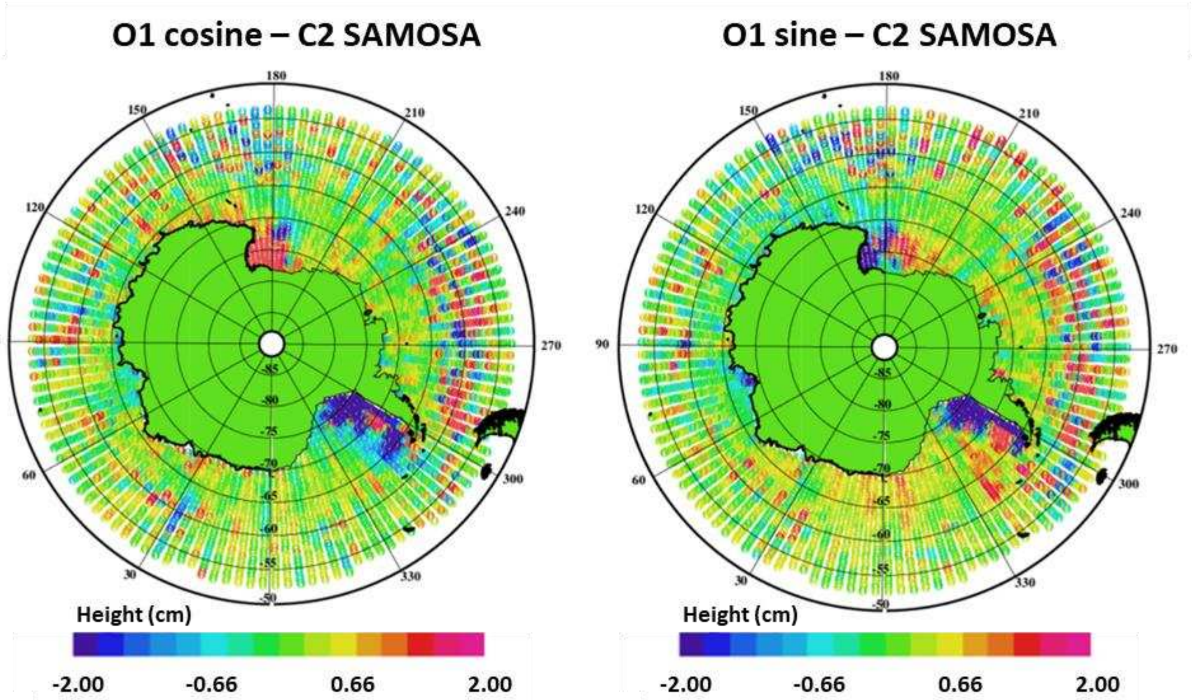


**Figure 9: The cosine and sine components of the O1 tidal residual estimated from CryoSat-2 data. Notice the colour scale is reduced to +/- 2 cm compared with previous plots.**

© NOVELTIS, DTU, UCL, NPI 2021
This document is the property of NOVELTIS, no part of it shall be reproduced or transmitted without the express prior written authorisation of NOVELTIS

# 3. Bathymetry improvement in the Southern Ocean

## 3.1. Analysis of existing bathymetry datasets (NOVELTIS)

### 3.1.1. Inventory of the bathymetry datasets

The work to be performed within the ALBATROSS project in order to improve the bathymetry in the Southern Ocean requires the identification of a relevant bathymetry dataset over the region, that will be used as prior solution.

A number of global and regional bathymetry datasets has been inventoried, providing various parameters (see Table 2).

As shown on Figure 10, the bathymetry is generally defined as the bedrock topography relative to chart datum (mean sea level, LAT – Lowest Astronomical Tides, local datum…), whatever the configuration (ocean or ice shelf).

However, the bathymetry information expected by the TUGO model, used to simulate the ocean tides, is the averaged free water layer thickness (“H model” on Figure 10).

Based on these definitions, only the bathymetry datasets that contain the necessary information to compute “H model” can be used under the ice shelves. This reduces the usable datasets to:

- the various releases of RTopo, for which the cavity geometry can be computed as the difference between the ice-base topography and the bedrock topography;
- BedMachine_Antarctica-2020-v2, for which the cavity geometry can be computed as the combination of ice surface elevation, ice thickness, and bedrock topography.

For all the other bathymetry datasets, some parameters are missing (in general, the ice thickness or the ice draft) to access the relevant information under the ice shelves. However, this does not prevent the use of these datasets outside the ice-shelf regions.

All these bathymetry products are generally provided with a grid giving the sources of the data that were used to build the bathymetry. For the older datasets, the information is sometimes only provided in the associated scientific publication.

Regarding the errors associated with these bathymetry datasets, there is generally no information, except for the BedMachine_Antarctica-2020-v2 dataset which comes with error estimates for the bed elevation and ice thickness in the same field (“errbed”).

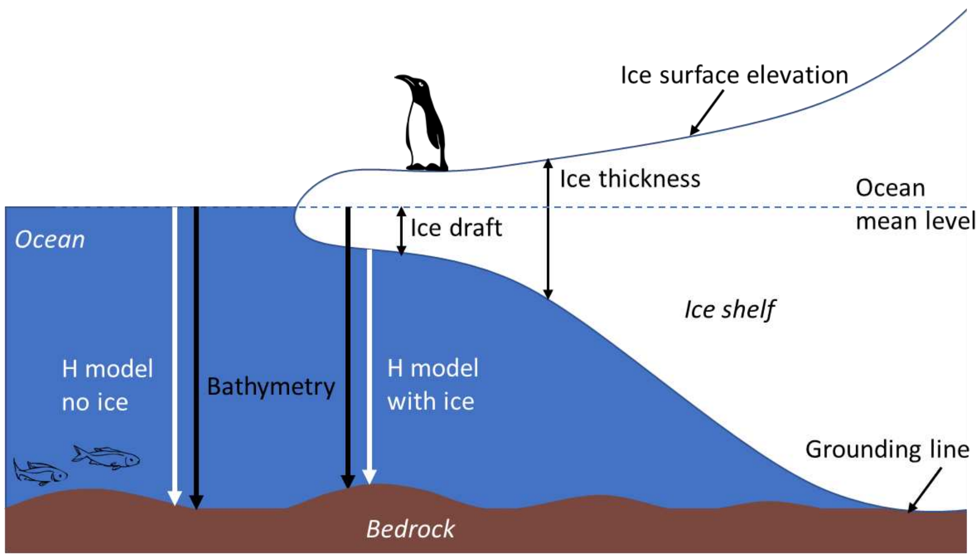


**Figure 10: Definitions of the quantities considered to determine the bathymetry and the free water column thickness expected by the TUGO model, in the ocean and under the ice shelves.**

© NOVELTIS, DTU, UCL, NPI 2021
This document is the property of NOVELTIS, no part of it shall be reproduced or transmitted without the express prior written authorisation of NOVELTIS

**Table 2: Inventory of global and regional bathymetry datasets available in the Southern Ocean.**

| Dataset | Resolution | Parameters | Backbone solution in the Southern Ocean | Reference |
|---|---|---|---|---|
| **IBCSO-v1** (2013)<br><br>Regional, up to 60°S | 1 minute | - Bedrock topography<br>- Ice surface elevation | GEBCO_08 | Arndt et al., 2013<br><br>https://doi.pangaea.de/10.1594/PANGAEA.805734?format=html |
| **BedMachine_Antarctica-2020-v2** (2020)<br><br>Regional, up to 60°S | Polar grid, close to 15 arcsec | - Bedrock topography<br>- Surface elevation<br>- Ice thickness | IBCSO-v1 | Morlighem et al., 2020<br><br>https://nsidc.org/data/NSIDC-0756/versions/2 |
| **RTopo-1.0.5b** (2010)<br><br>Global | 1 minute | - Bedrock topography<br>- Ice-base topography (= ice draft for ice shelves)<br>- Surface elevation<br>- Coastline<br>- Grounding line | s-2004<br><br>ALBMAP-v1 | Timmermann et al., 2010<br><br>https://doi.pangaea.de/10.1594/PANGAEA.741917?format=html#download |
| **RTopo-2.0.1** (2016)<br><br>Global | 30 arcsec | - Bedrock topography<br>- Ice-base topography (= ice draft for ice shelves)<br>- Surface elevation<br>- Ice thickness<br>- Coastline | IBCSO-v1 | Schaffer and Timmermann, 2016<br><br>https://doi.pangaea.de/10.1594/PANGAEA.856844?format=html#download |
| **RTopo-2.0.4** (2019)<br><br>Global | 30 arcsec | - Bedrock topography<br>- Ice-base topography (= ice draft for ice shelves)<br>- Surface elevation<br>- Ice thickness<br>- Coastline<br>- Grounding line | IBCSO-v1 | Schaffer et al., 2019<br><br>https://doi.pangaea.de/10.1594/PANGAEA.905295?format=html#download |
| **GEBCO-2020** (2020)<br><br>Global | 15 arcsec | - Bathymetry | IBCSO-v1 | https://www.gebco.net/data_and_products/gridded_bathymetry_data/gebco_2020/ |
| **GEBCO-2021** (2021)<br><br>Global | 15 arcsec | - Bathymetry<br>- Ice surface elevation<br>- Under-ice bedrock elevation | IBCSO-v1<br><br>Bedmachine_Antarctica-2020-v2 (under ice) | https://www.gebco.net/data_and_products/gridded_bathymetry_data/ |

© NOVELTIS, DTU, UCL, NPI 2021
This document is the property of NOVELTIS, no part of it shall be reproduced or transmitted without the express prior written authorisation of NOVELTIS

The definition of the free water column layer thickness under the ice shelves is crucial to obtain accurate tidal simulations, not only in the Southern Ocean, but even at the global ocean scale. Figure 11 shows the dramatic impact of the choice of bathymetry under the ice shelves in Antarctica, in the case of a global hydrodynamic simulation (work performed within the CNES/CLS/NOVELTIS/LEGOS FES2022 project, Carrère et al., 2020). Using the GEBCO-2020 bathymetry information under the ice shelves strongly degrades the tidal solution everywhere in the global ocean, with errors to altimetry observations that are more than doubled compared to the simulation where the relevant height information is used (RTopo-2.0.4 in this case).

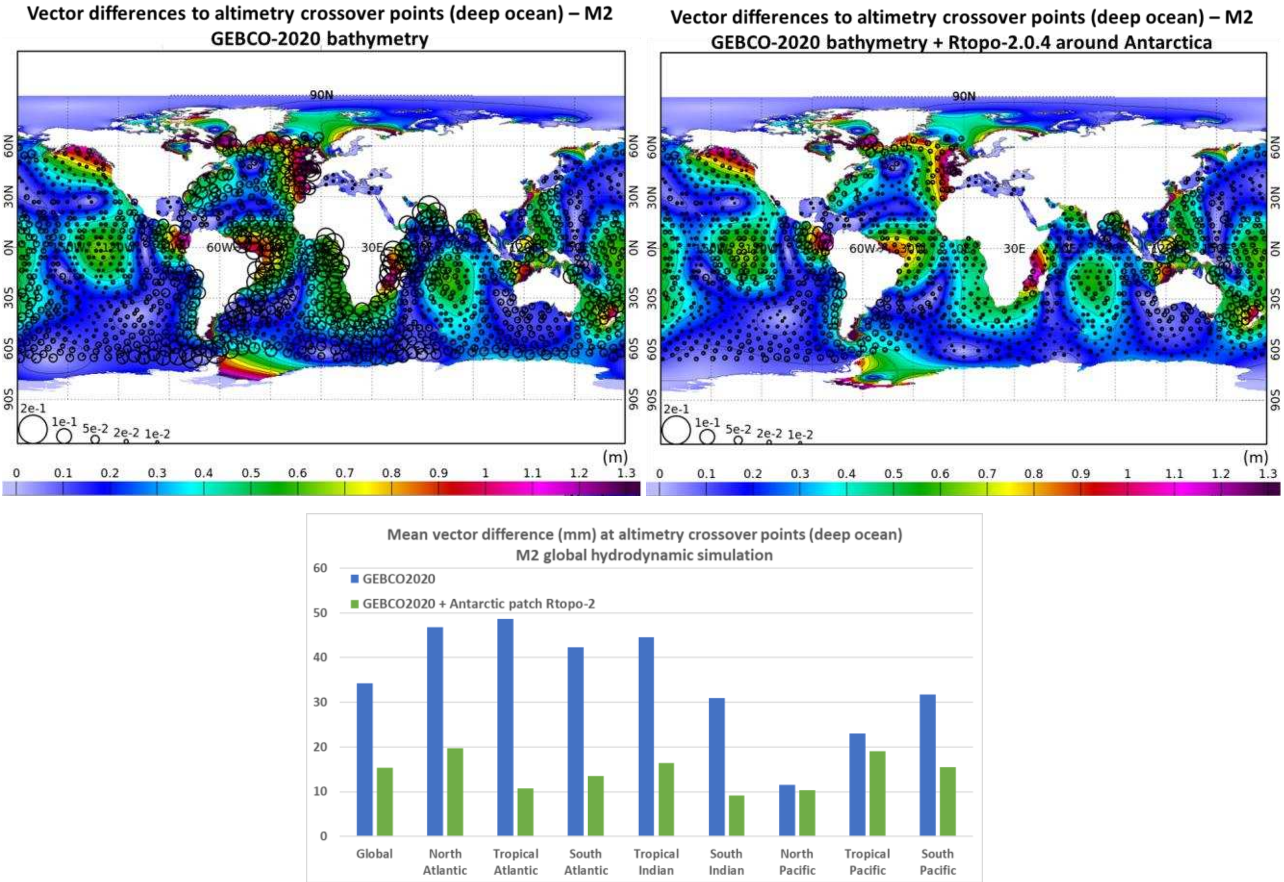


**Figure 11: Upper plots: Global hydrodynamic simulation of the M2 tidal component (background colours show the amplitude in m) based on the GEBCO-2020 bathymetry (left) or the combination of GEBCO-2020 and RTopo-2.0.4 in the Southern Ocean (right). The size of the black circles (in m) is proportional to the vector difference between the model and the tidal observations derived from altimetry crossover points. Lower plot: Vector differences on the M2 tidal component between the altimetry crossover points and each of the two tidal simulations, for the global ocean and per basin. (Courtesy FES2022 project)**

Another important aspect to consider is the fact that all these bathymetry datasets are strongly linked to each other, as some are used as the backbone solution of the others, and some regional solutions have been merged into global ones (see Table 2).

Figure 12 and Figure 13 respectively show the differences (absolute and relative) between GEBCO-2021 and RTopo-2.0.4, and BedMachine_Antarctica-2020-v2 and RTopo-2.0.4, in the Southern Ocean. Apart from the ice-shelf regions, where the information provided in each dataset is not the same, as explained above, the main differences between GEBCO2021 and RTopo-2.0.4 are located in the deep ocean, North of 60°S. In the seasonally sea-ice covered region comprised between 60°S and the Antarctica shoreline, the differences are much smaller, probably due to the lack of observations in both datasets.

On the contrary, the main differences between RTopo-2.0.4 and BedMachine_Antarctica-2020 are located under the ice shelves and very close to the coast. Everywhere else, the two datasets are almost similar, as they are both based on IBCSO-v1 (cf. Table 2). The only noticeable offshore differences are located at the continental shelf break and in regions of steep topography gradients, and they are due to the different resolutions of the bathymetry grids (30 arcsec for RTopo-2.0.4; 15 arcsec for BedMachine_Antarctica-2020).


© NOVELTIS, DTU, UCL, NPI 2021
This document is the property of NOVELTIS, no part of it shall be reproduced or transmitted without the express prior written authorisation of NOVELTIS

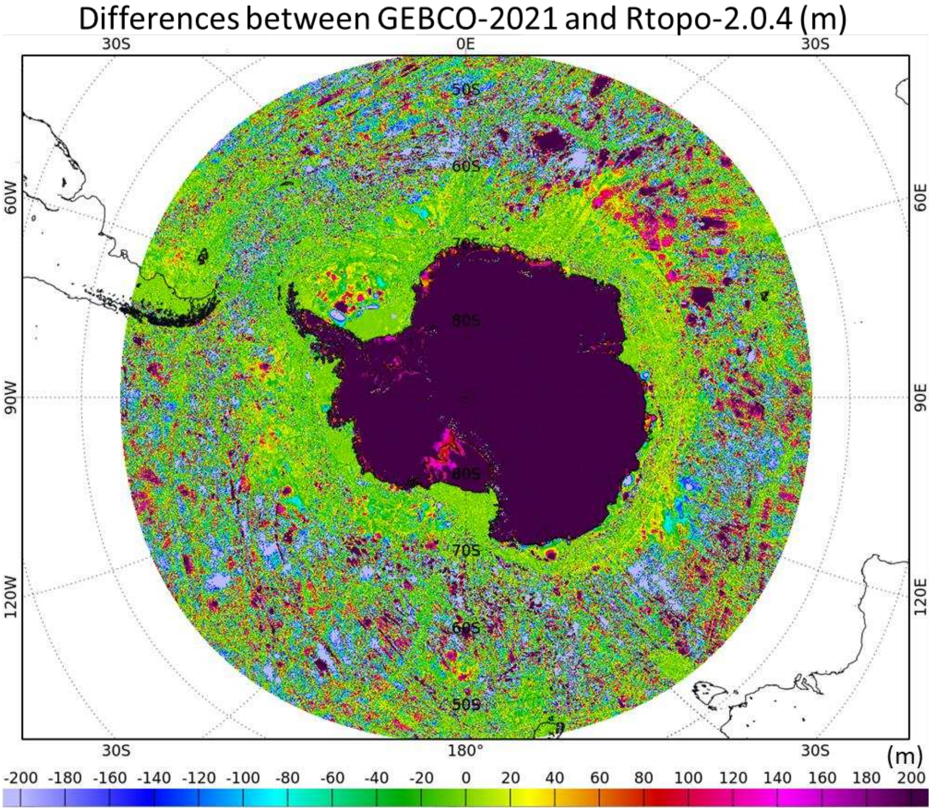


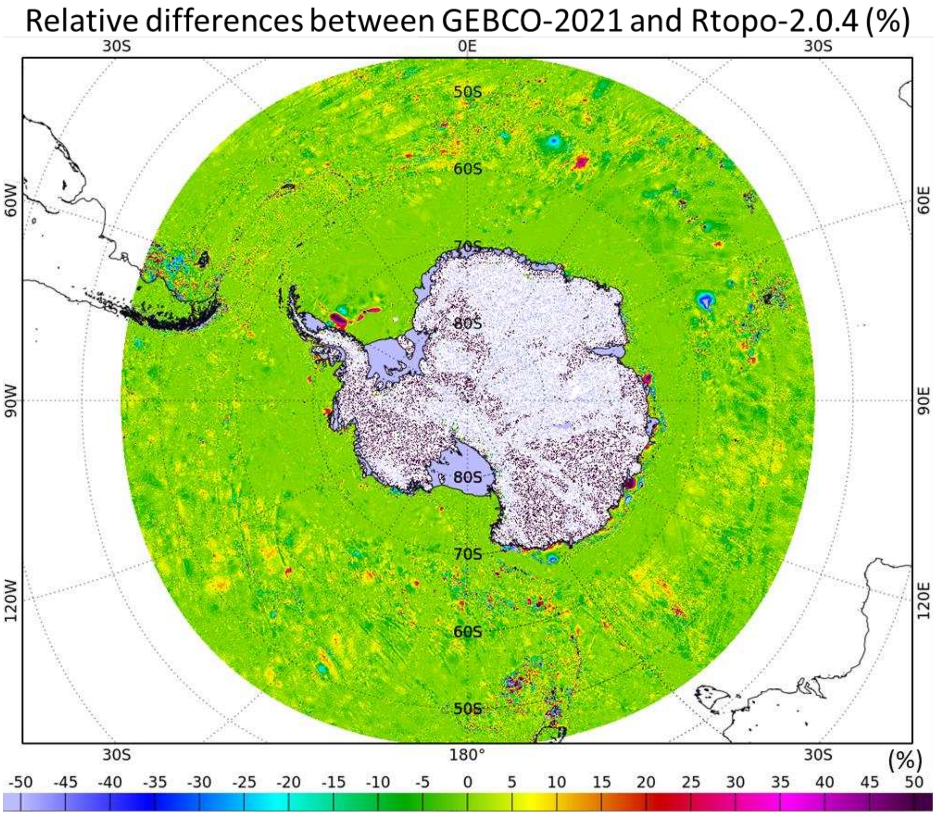


**Figure 12: Absolute (upper plot, in meters) and relative (bottom plot, in percentage) differences between the GEBCO-2021 and RTopo-2.0.4 bathymetry datasets in the Southern Ocean.**

© NOVELTIS, DTU, UCL, NPI 2021
This document is the property of NOVELTIS, no part of it shall be reproduced or transmitted without the express prior written authorisation of NOVELTIS

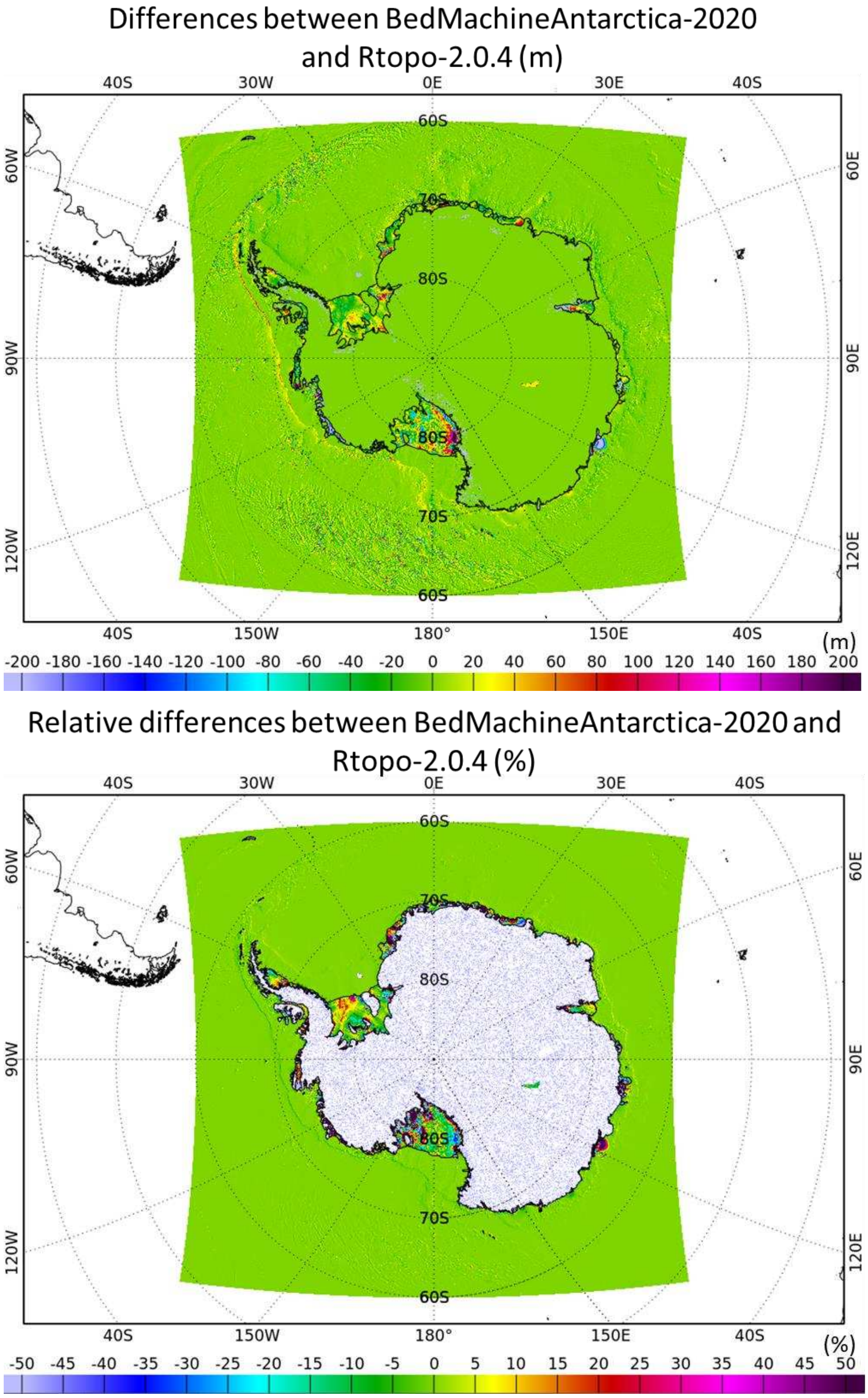


**Figure 13: Absolute (upper plot, in meters) and relative (bottom plot, in percentage) differences between the BedMachine_Antarctica-2020-v2 and RTopo-2.0.4 bathymetry datasets in the Southern Ocean.**


© NOVELTIS, DTU, UCL, NPI 2021
This document is the property of NOVELTIS, no part of it shall be reproduced or transmitted without the express prior written authorisation of NOVELTIS

### 3.1.2. Identification of the reference bathymetry dataset

In order to select a prior bathymetry dataset for the improvement work to be performed within the ALBATROSS project, the various available datasets have been considered and compared. As previously mentioned, for the ice-shelf regions, which are crucial areas to generate accurate tidal simulations, the choice is limited to the RTopo global datasets and to the BedMachine_Antarctica-2020-v2 regional dataset. In terms of grid resolution and consistency with recent coastlines (GSHHS-2.3.7 in particular), the RTopo-2.0.4 global dataset appears to be the most relevant compared to the other releases of this family. It was thus compared to the BedMachine_Antarctica-2020-v2 regional dataset.

Because of the high sensitivity of the tidal model to the bottom topography, a way to assess the bathymetry datasets consists in evaluating how they impact hydrodynamic tidal simulations. The TUGO hydrodynamic model was thus run using the regional configuration described in section 2.1, for each bathymetry dataset.

The BedMachine_Antarctica-2020-v2 bathymetry coverage is limited to 60°S in part of the Southern Ocean, which does not cover the whole model regional domain. In order to fill the gaps, the BedMachine_Antarctica-2020-v2 bathymetry was merged into the RTopo-2.0.4 global dataset. The resulting bathymetry at 15 arcsec is noted BedMachine+RTopo-2.0.4 hereinafter.

Figure 14 shows the impact of the choice of bathymetry on the regional tidal simulations, through the comparison with coastal tide gauge observations and GPS stations located in the ice-shelf regions (database from Howard et al., 2020). Indeed, as shown in Figure 13, the main differences between the two bathymetry datasets are located along the Antarctica coast and under the ice shelves.

The largest differences between the two tidal hydrodynamic simulations are located in ice-shelf regions, namely the Filchner-Ronne ice shelf, in the Weddell Sea, and the Amery ice shelf, in east Antarctica. In general, using the BedMachine_Antarctica-2020-v2 bathymetry dataset reduces the errors of the tidal hydrodynamic simulation to the coastal and ice-shelf observations around the Antarctic Peninsula, in the Weddell Sea and in the Ross Sea, compared to the simulation based on RTopo-2.0.4. The only large degradation observed with the BedMachine_Antarctica-2020-v2 dataset is located at a GPS station on the Amery ice shelf. However, this specific region, as well as the bays under the Filchner-Ronne ice shelf where the largest differences to observations are noted, whatever the simulation, will be more closely investigated during the project (see section 3.5).

Following these analyses, the BedMachine_Antarctica-2020-v2 dataset was selected as the reference bathymetry for the bathymetry work within the ALBATROSS project. To cover the whole domain, we use the combination with RTOPO-2.0.4, i.e. the BedMachine+RTopo-2.0.4 dataset.

© NOVELTIS, DTU, UCL, NPI 2021
This document is the property of NOVELTIS, no part of it shall be reproduced or transmitted without the express prior written authorisation of NOVELTIS

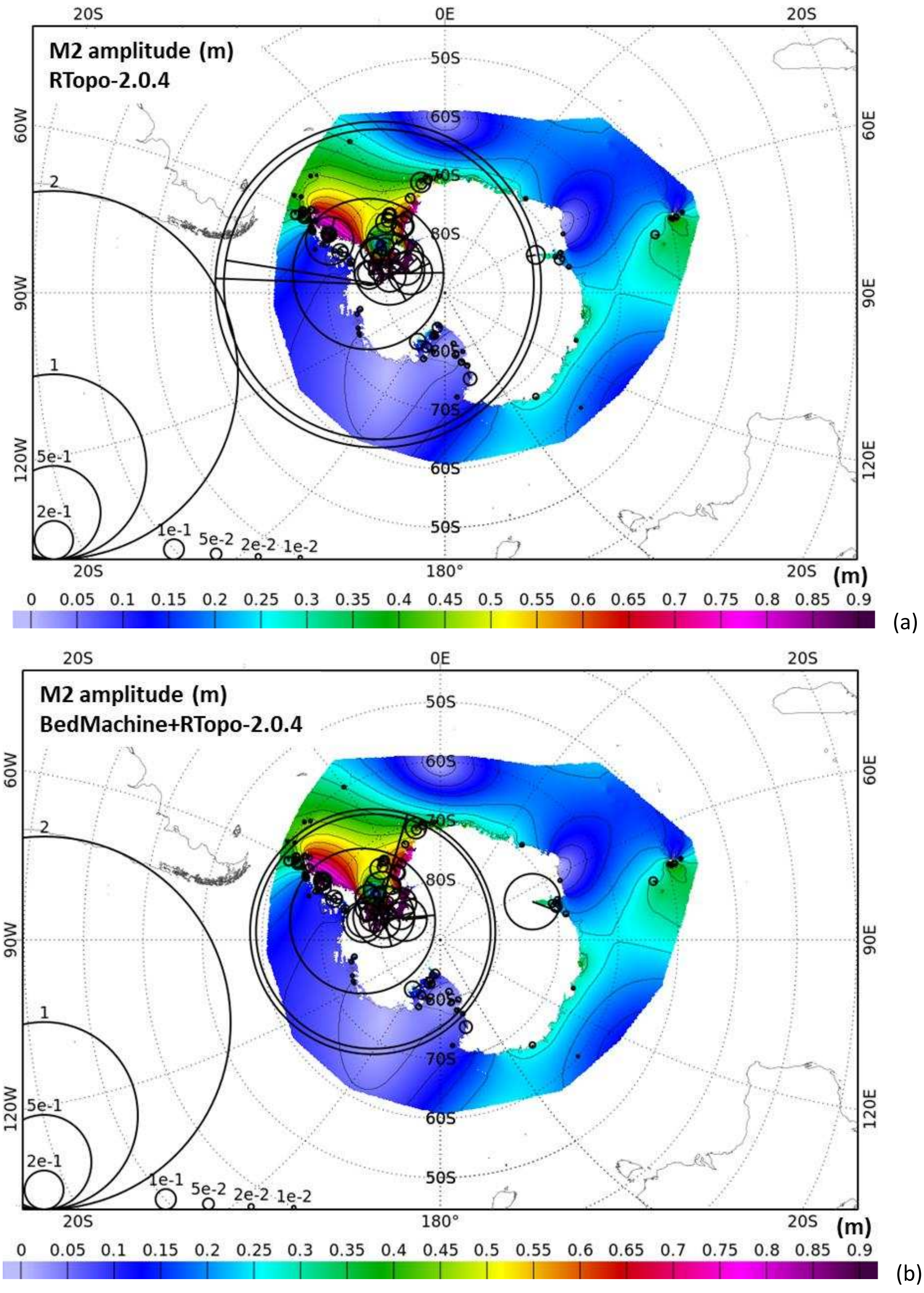


**Figure 14: Regional hydrodynamic simulations of the M2 tidal component (background colours show the amplitude in m) based on the RTopo-2.0.4 bathymetry (a) and on the combination of BedMachine_Antarctica-2020-v2 and RTopo-2.0.4 (b). The size of the black circles is proportional to the vector difference (in m) between the model and the tidal observations derived from tide gauges and GPS stations.**

© NOVELTIS, DTU, UCL, NPI 2021
This document is the property of NOVELTIS, no part of it shall be reproduced or transmitted without the express prior written authorisation of NOVELTIS

## 3.2. Bathymetry improvement in the deep ocean (DTU)

The existing bathymetry map of the Southern Ocean is a compilation of ship soundings. Due to the presence of all-year sea ice, costly operations and political restrictions, dense and full coverage of the Southern Ocean is not possible, leaving huge gaps between the existing surveys. In this investigation, we make use of the combination of the BedMachine_Antarctica-2020-v2 and RTopo-2.0.4 bathymetry datasets merged by NOVELTIS in the Southern Ocean as described in section 3.1.2 (hereinafter called the BedMachine+RTopo-2.0.4 bathymetry), and we perform an inversion to derive an enhanced Southern Ocean bathymetry using the recent altimetric gravity model DTU21GRA. This gravity field is significantly improved with revised data processing strategy of the CryoSat-2 data using the SAMOSA+ retracker. In the derivation of DTU21GRA, sea level anomalies with respect to the EGM2008 geoid are processed in tiles of 1 x 3 degrees. DTU21GRA is based on all geodetic mission data (CryoSat-2, Saral and Jason-1 and 2). SAMOSA+ has only been used in Polar regions outside the 60 parallels and only CryoSat-2 SAR and SARin data from SAMOSA+ have been used. Initially, the SAMOSA+ data are used to compute 2-Hz sea level anomalies and then these data are merged with data from other geodetic missions. These are subsequently iteratively processed. In this iterative process, the data are crossover-adjusted to remove long wavelength and then edited based on 2.5 times the local standard deviation of the data. Subsequently this reduced dataset is submitted to a new crossover adjustment and editing until no further data are removed. Typically, this removed between 3 and 6 percent of the data in up to 10 iterations. The final dataset is then submitted to a gravity field prediction procedure using FFT techniques and the EGM2008 gravity field restored to derive DTU21GRA.

The long and short wavelength components are preserved from the BedMachine+RTopo-2.0.4 bathymetry. The band-pass filtering function proposed by Smith and Sandwell (1994) is updated for the Southern Ocean by reducing the cut-off wavelength similarly to the work presented in Abulaitijiang et al. (2020).

The predicted bathymetry can be written as the sum of the long wavelength component of the input bathymetry, the inverted topography from band-pass filtered gravity and the remaining short-wavelength components from the high-pass filter of the input bathymetry, as below:

$$H_p(x) = B_{long}(x) + S(x) \cdot G_{BP}(x) + B_{short}(x) \quad \text{(Eq. 1)}$$

where S(x) is the scaling factor used to convert gravity to topography, with unit m/mGal.

We present the BedMachine+RTopo-2.0.4 bathymetry high-pass filtered at 20 km and low pass filtered at 60 km in Figure 15. These latter represent the $B_{short}$ and $B_{long}$ contributions in the equation above. The scale is given in meters.

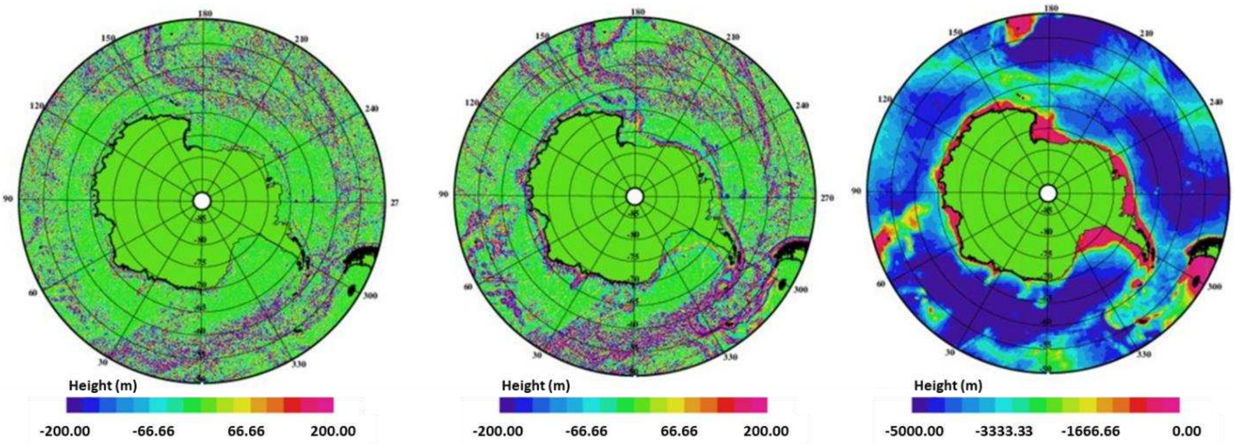


**Figure 15: BedMachine+RTopo-2.0.4 bathymetry high-pass filtered at 20 km (left), band-passed filtered at 20-60 km (middle) and low-pass filtered at 60 km (right). These high- and low-pass sections represent the $B_{short}$ and $B_{long}$ contributions in the equation above. The band-pass central picture is the one being replaced using the inversion of the gravity field. The scale is given in meters.**

© NOVELTIS, DTU, UCL, NPI 2021
This document is the property of NOVELTIS, no part of it shall be reproduced or transmitted without the express prior written authorisation of NOVELTIS

The band-pass filtering function proposed by Smith and Sandwell (1994) is referred to as Smith&Sandwell (S&S) filter in the following sections. The general form is:

$$W(k) = W_1(k) \cdot W_2(k) \cdot exp[2\pi kd] \quad \text{(Eq. 2)}$$

Where $W_1(k)$ is a high-pass Gaussian filter; $W_2(k)$ is a low-pass filter, the exponential term is the downward continuation operator, in which *d* is the depth in km, and *k* is the wavenumber with unit km$^{-1}$.

The forms are:

$$W_1(k) = 1 - exp[-2(\pi ks)^2],$$
$$W_2(k) = \{1 + Ak^4 exp\,[4\pi kd]\}^{-1}.$$

The *s* parameter in W1(k) is the Gaussian parameter (s=20 km) with assumed crust thickness of 7 km; the *A* parameter in W2(k) is a constant chosen by the spectral coherence (between bathymetry and gravity); W1(k) is a function of depth, and in the deeper ocean depths, the gravity signal is suppressed by this filter at "longer" wavelengths, compared to that of shallow sea floor.

The 20-km high-pass filtered version of the BedMachine+RTopo-2.0.4 bathymetry is kept at 15 arc second resolution to maintain the high frequency short wavelength signals. The remaining band-passed and low-pass filtered bathymetry is subsampled at 1 minute (using spline interpolation) as this does not degrade the signal contents.

DTU21GRA is the most recent global marine gravity field from DTU Space (Andersen et al., 2021). It is shown in Figure 16 (left), to be compared with the BedMachine+RTopo-2.0.4 bathymetry (right) band-filtered between 20 and 60 km. Scale is mGal for the DTU21GRA gravity field and meters for the BedMachine+RTopo-2.0.4 bathymetry. In order to make the two figures appear similar, the scaling of the bathymetry is roughly 10 times that of the gravity. When inspecting the two fields, there are regions close to Antarctica where there is a stronger signal in the gravity than in the bathymetry. There is a particular fracture zone related feature at 58S-60S and 50E which seems extended in the gravity field but not in the bathymetry.

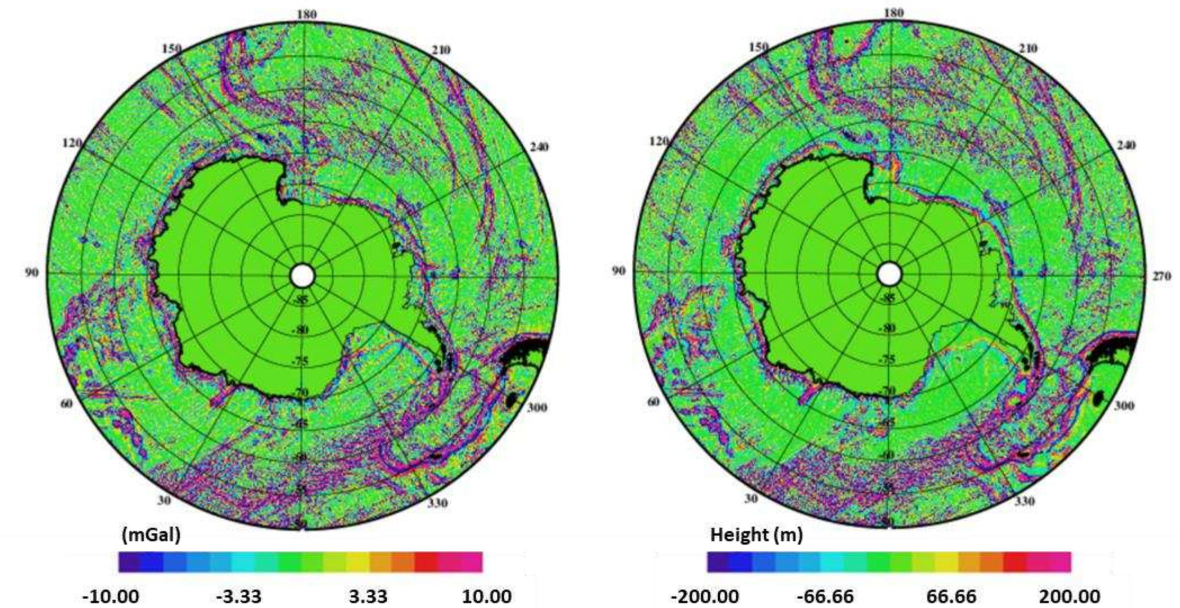


**Figure 16: DTU21GRA gravity field (left) and BedMachine+RTopo-2.0.4 bathymetry (right) band-filtered between 20 and 60 km. Scale is mGal for DTU21 Gravity and meters for BedMachine+RTopo-2.0.4 bathymetry.**

© NOVELTIS, DTU, UCL, NPI 2021
This document is the property of NOVELTIS, no part of it shall be reproduced or transmitted without the express prior written authorisation of NOVELTIS

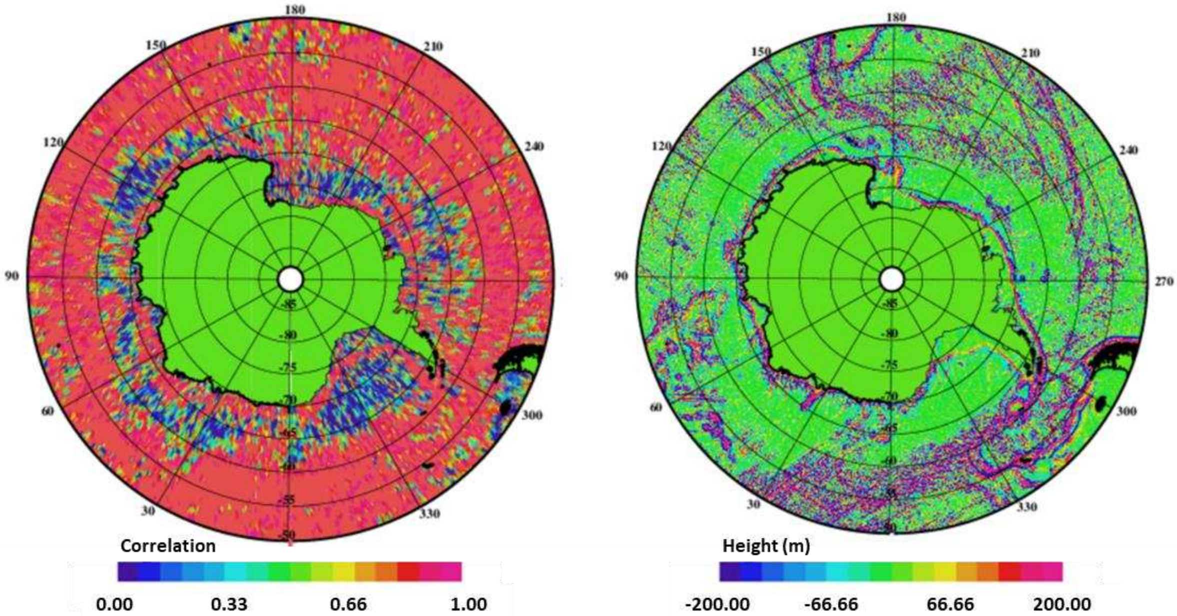


**Figure 17: The spatial correlation between the band-pass filtered (20-60 km) DTU21 gravity field and the BedMachine+RTopo-2.0.4 bathymetry (left), and the 20-60 km band-pass filtered BedMachine+RTopo-2.0.4 bathymetry (right).**

The spatial coherency computed along with the spatial correlation is used to determine the scaling factor for each 1-degree block. The unfiltered and filtered versions of this are shown in Figure 18 in the left and right panel respectively.

The computation of the resulting bathymetry is still on-going.

The ALES+ SAR processing developed during the Baltic+SEAL project (http://balticseal.eu/) could be tested for gravity field prediction. We have not currently done so and this is outside the scope of this project. Also, the Baltic+SEAL data do not include SARin processed data, which are mandatory to get close to the coast of Antarctica. However, it would be very interesting to include a fully processed ALES+ dataset in the Polar regions in an updated release of the DTU gravity field.

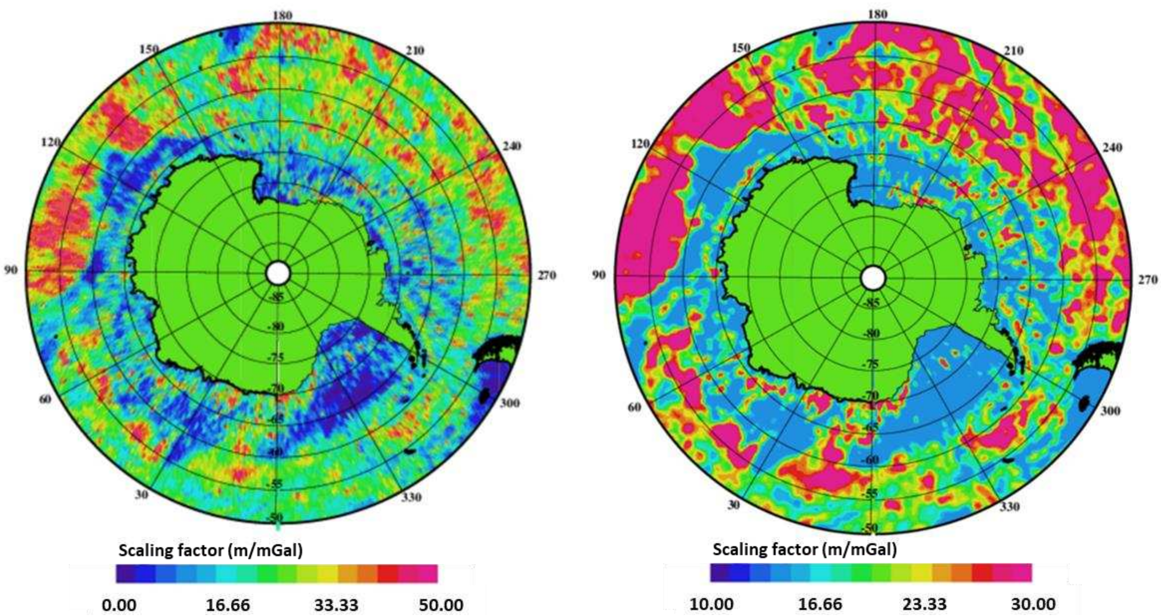


**Figure 18: The unfiltered (left) and filtered (right) scaling factors for the equation above. The unit of the scaling factor is m/mGal. Notice that the scales are different for the unfiltered and filtered scaling factors.**


© NOVELTIS, DTU, UCL, NPI 2021

This document is the property of NOVELTIS, no part of it shall be reproduced or transmitted without the express prior written authorisation of NOVELTIS

### 3.3. Sea ice surface characteristics to improve bathymetry gradient location (UCL)

Figure 19 illustrates the general workflow methodology used in model generation to retrieve the sea ice surface roughness characteristics from MISR reflectance observations.

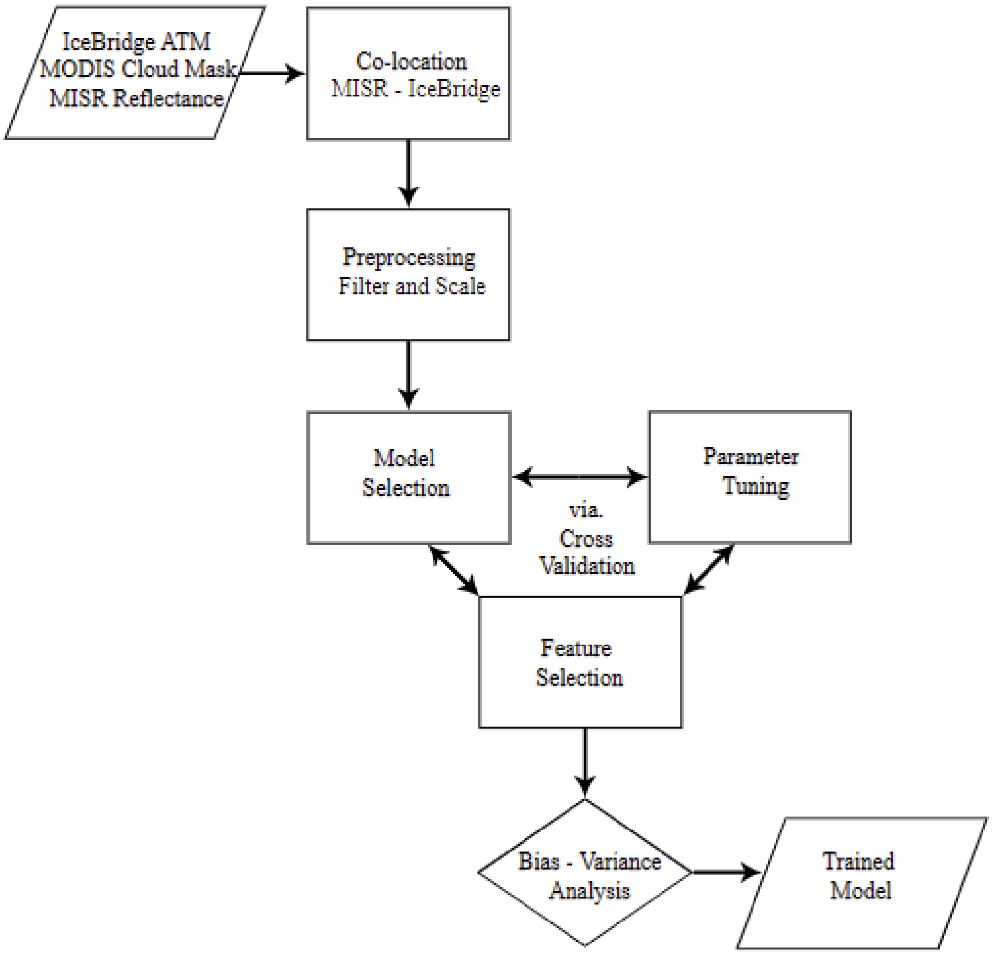


**Figure 19: A process diagram illustrating the workflow methodology used in model generation. Note that model selection, feature selection, and hyper-parameterization constitute an iterative process that converges on a final hyper-parameterized model and feature subset via cross validation. Credit: Johnson et al (2022).**

The Figure 20 illustrates the typical OIB airborne laser elevation data (~200 m by 1 km) used to train the MISR roughness algorithm. This example contains a lead (blue low elevation region and first peak in the PDF) as well as sea ice features such as level ice and ridges. The roughness is defined as the standard deviation of the PDF shown on the left. At present no special treatment is done to remove leads from the analysis or to detect leads as part of the algorithm, and the roughness captures the entire topography of the scene that is sampled (Johnson et al., 2021).

As suggested by our ESA colleagues, for altimetry data, L1b waveforms are typically classified using neural networks and also retrackers can support the selection of the data with their output (sigma-0, swh/mss…). Here, we anticipate that in a second version of our roughness product we will distinguish lead features (blue region in Figure 20) from sea ice elevations using a surface classification approach already implemented for the Arctic (Kurtz et al., 2013) and more recently for the Antarctic (Mei and Maksym, 2020). We do not consider this to be critical for the characterization of sea ice surface roughness for this project as smoother surfaces are already detectable even with the current implementation of the algorithm.

© NOVELTIS, DTU, UCL, NPI 2021
This document is the property of NOVELTIS, no part of it shall be reproduced or transmitted without the express prior written authorisation of NOVELTIS

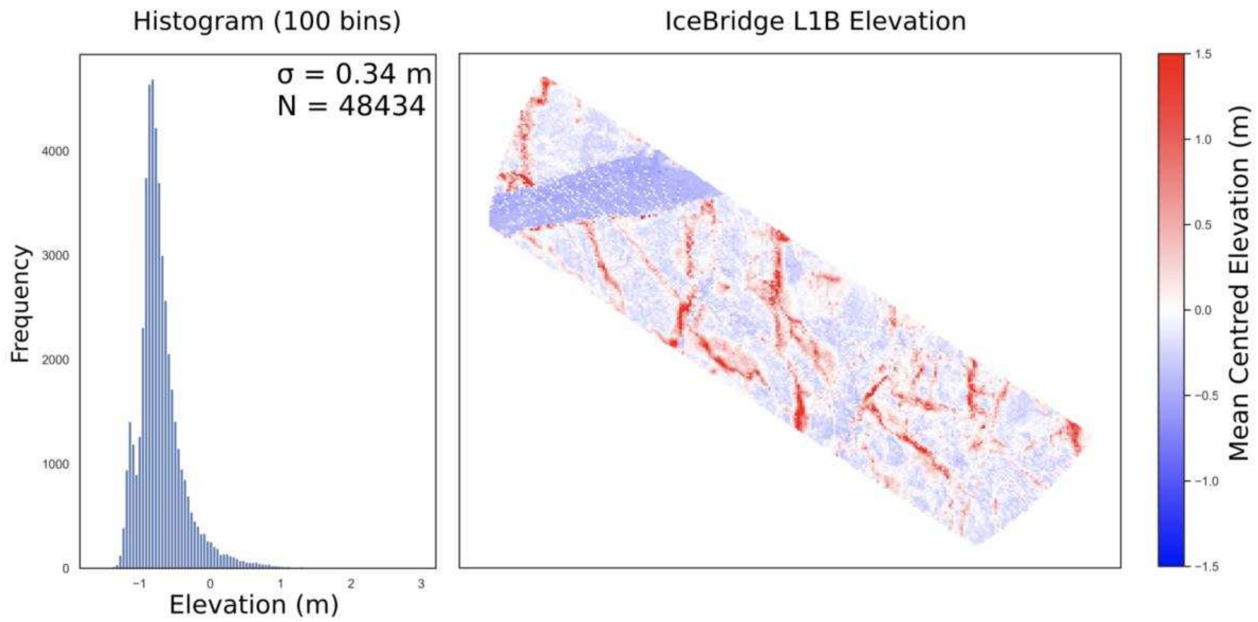


**Figure 20: The derivation of surface roughness centred on a MISR pixel from coincident elevation measurements: (left) PDFs of elevation used to derive surface roughness used in training, (right) within MISR pixel footprint of elevation measurements**

We have processed all the L1b OIB ATM Antarctic data and collocated them with MISR swaths yielding 10000s of training instances at the 1.1 km MISR grid resolution. Note that OIB data in Antarctica have not been processed yet by NASA to a higher-level product and this is one of the first example of use of these very useful datasets.

We have now generated version 1 of the Antarctica MISR roughness algorithm and it is being applied to entire MISR images. This process is lengthy as it requires tens of Tb of MISR and MODIS (for cloud mask and surface temperature auxiliary fields) to be downloaded and processed on our servers. We have processed to date 1 year of data (Figure 21, c). The year 2017 was chosen as it contains a polynya opening over Maud Rise in the Weddell Sea, which is a striking example of the coupling between ocean, bathymetry and sea ice in the Southern Ocean (Jena et al, 2019).

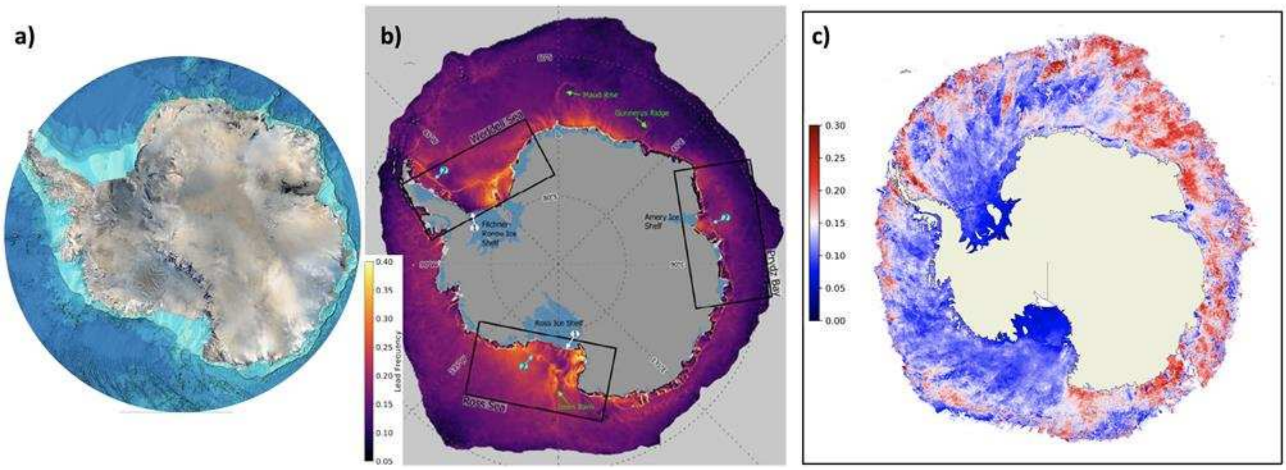


**Figure 21: a) GEBCO Antarctica and Southern Ocean topography. b) Lead frequency average from 16 years (2003-2018) of winter (April-September) MODIS thermal infrared satellite data (Reiser et al, 2020). c) Mean roughness mosaic from one year of MISR data (Johnson et al, 2022).**

We are also processing 10 years of spring data (to be extended to 20 years in a second stage) to generate sufficient statistics to identify surface signatures of bathymetry gradients. This approach was proposed by Reiser et al. (2020) using 16 years of Winter MODIS data to identify lead frequency. Here we go a step further and by tracking the frequency of smooth data we expect to have a more accurate identification of surface signature of bathymetry triggered events such as for example tidally generated enhanced vertical heat fluxes at the bathymetry slope (Hannah et al, 2009).


© NOVELTIS, DTU, UCL, NPI 2021
This document is the property of NOVELTIS, no part of it shall be reproduced or transmitted without the express prior written authorisation of NOVELTIS

Preliminary encouraging results have shown in the Arctic that the MISR roughness products are strongly correlated with the ice thickness from both CryoSat-2 (above ~0.5m) and SMOS (below ~0.5m). The next steps consist in i) producing 10 years (and up to 20 years) of sea ice roughness data from MISR to have enough statistics to ii) identify regions of frequent low roughness/thickness sea ice in order to iii) correlate these with bathymetry features and tidal signal to eventually produce iv) a regression model of bathymetry as a function of tidal signal and sea ice surface signature that could be in turn used to v) refine the location over the bathymetry slope regions in poorly sampled Southern Ocean regions.

© NOVELTIS, DTU, UCL, NPI 2021
This document is the property of NOVELTIS, no part of it shall be reproduced or transmitted without the express prior written authorisation of NOVELTIS

## 3.4. Data collection for ice shelves (NPI)

Knowledge of bathymetry under the ice shelves is limited to scattered observation campaigns with autonomous underwater vehicles, seismic surveys on the ice and airborne gravity from which bathymetry can be inverted. In between these areas, synthetic data needs to be generated. In the BEDMAP-1 compilation (Lythe et al., 2001), data gaps under the ice shelves were filled with a bicubic spline interpolation between the grounding line and the seabed outside the ice-shelf front. This basic interpolation has remained a baseline dataset for more recent bathymetry products even if newer bathymetry observations have been implemented. Examples of such inherited bathymetry products are BEDMAP-2, RTopo-1/2, GEBCO/IBCSO, and the most recent compilation, BedMachine_Antarctica (Morlighem et al., 2020).

We use BedMachine_Antarctica as a starting point for continuous bedrock heights under the ice-sheet and the ice shelves, and then improve it in the coastal zone by adding regional bathymetry compilations from more recent studies (e.g. Eisermann et al., 2020; Smith et al., 2020). We then cut away areas where the ice sheet is grounded by applying a combined grounding line from Gardner et al. (2018) and Matsuoka et al. (2015), which we further refine with more recent data from SAR interferometry and satellite altimetry. This provides the starting point for further analysis of water column thickness, which is what matters for a tide model, but is typically not available as a separate data product.

We derive an initial grid of water column thickness at 1 km resolution by following these steps:

- Calculate ice-shelf freeboard by subtracting a geoid model (EIGEN; Foerste et al., 2014) and the mean ocean topography (DTU; Andersen and Knudsen, 2009) from the Reference Elevation Model of Antarctica (REMA; Howat et al., 2019). We define the inland ice-shelf extent by our refined grounding line, and the coastal extent by REMA itself, setting an elevation cut-off of 10 m above sea level.
- Calculate ice-shelf thickness from the ice-shelf freeboard by applying a firn density model (Ligtenberg et al., 2011) and assuming hydrostatic equilibrium.
- Calculate ice-shelf draft by subtracting the ice thickness from the surface elevations of REMA.
- Calculate water column thickness from the difference between the ice-shelf draft and the bathymetry.

Since bathymetry and ice-shelf draft are derived from independent data, there are areas where the draft is estimated to be deeper than the bathymetry which is not possible. In those cases, we investigate which data source is most likely to be in error (usually the bathymetry) and adjust accordingly. The REMA model itself gives a good indication whether an area might be grounded through a local rise in elevation or visible surface scars and rifting in hill-shade plots. We further use this to map out other small ice rumples and pinning-points which have not been detected in the grounding line mapping. These areas are added to the grounding line product and set to zero water column thickness. In cases where the gradient becomes unrealistically steep, nearby data (5-10 km) are deleted and re-interpolated.

Beyond the ice shelves, one can also use high-resolution satellite data to detect grounded icebergs which give a further constraint on local bathymetry. If an iceberg appears at the same spot in repeated imagery and is not trapped in fast ice, then one can assume that it is grounded. By assuming a typical iceberg freeboard, the minimum local bathymetry can be calculated as the inferred ice draft from hydrostatic inversion, as done for the ice shelves. This is done for a distance up to 50 km from the ice-shelf front although most grounded icebergs are located much closer. Similar as for the ice shelves, unrealistically steep bathymetry gradients are corrected by nearby data removal and re-interpolation.

The main end-product to be used further within ALBATROSS is a set of points at 1 km posting covering the ice-shelf extents and seamlessly connecting to the open ocean over a 50 km distance from the fronts. These points have three parameters; 1) ice shelf draft (zero elsewhere), 2) bathymetry, and 3) water column thickness (bathymetry minus draft). These point data are to be implemented in the bathymetry meshing of WP 1.4.

© NOVELTIS, DTU, UCL, NPI 2021
This document is the property of NOVELTIS, no part of it shall be reproduced or transmitted without the express prior written authorisation of NOVELTIS

## 3.5. Integration of the bathymetry datasets (NOVELTIS)

In parallel to the work performed for the deep ocean (§3.2), the bathymetry gradient location (§3.3) and the ice shelves (§3.4), further analyses have been performed on the tidal simulations based either on the BedMachine_Antarctica-2020-v2 bathymetry or on the RTopo-2.0.4 bathymetry (see §3.1.2).

Indeed, if the choice of the BedMachine_Antarctica-2020-v2 dataset as the general reference bathymetry seems the most relevant, the results can be more contrasted locally.

We present here some analyses under the Filchner-Ronne ice shelf in the Weddell Sea, and under the Amery ice shelf in east Antarctica.

### 3.5.1. Case of the Filchner-Ronne ice shelf (Weddell Sea)

The vector differences at some of the GPS observations located on the Filchner-Ronne ice shelf are particularly large for the two regional simulations based either on BedMachine_Antarctica-2020-v2 or RTopo-2.0.4, especially in the Rutford Ice Stream (see Figure 22 for the local toponyms). The differences to these GPS stations are much smaller in the case of the FES2014 purely hydrodynamic tidal solution (before data assimilation), as shown in Figure 23, although the FES2014 model is not defined as deep in the bays as the regional model, and its mesh is much coarser in the area. The bathymetry used in the Southern Ocean to produce the FES2014 model was RTopo-1.0.5b.

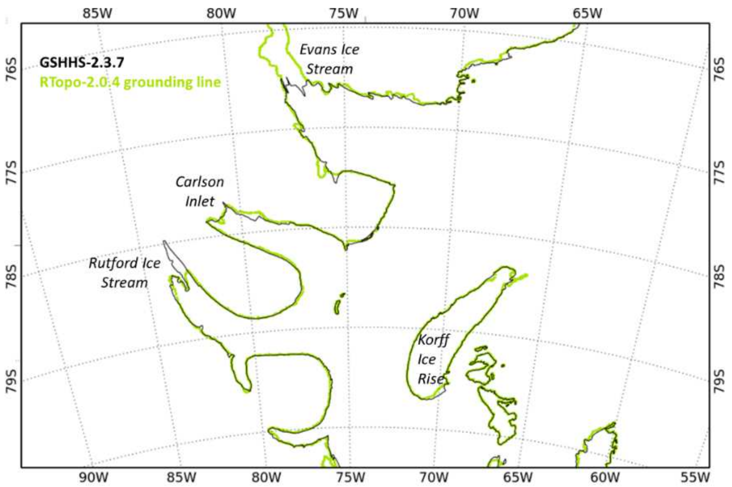


**Figure 22: GSHHS-2.3.7 coastline and RTopo-2.0.4 grounding line in the western part of the Filchner-Ronne ice shelf, in the Weddell Sea**

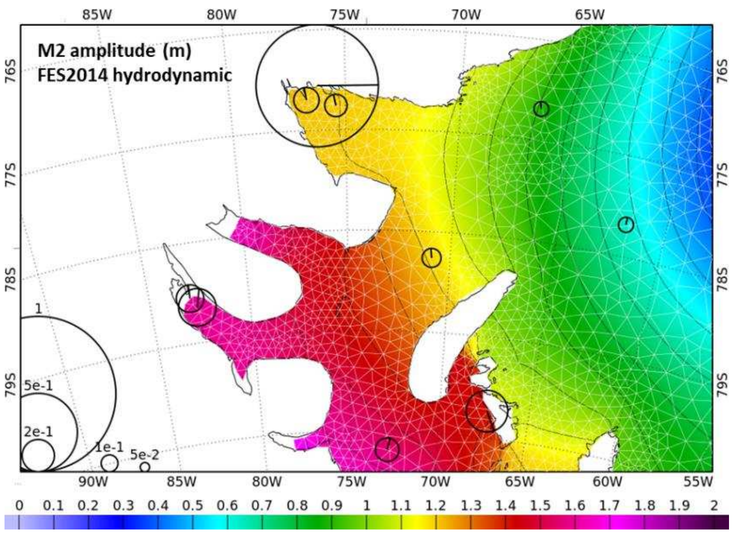


**Figure 23: FES2014 hydrodynamic simulation of the M2 tidal component (background colours show the amplitude in m) under the Filchner-Ronne ice shelf. The size of the black circles is proportional to the vector difference (in m) between the model and the in-situ observations. The FES2014 model mesh grid is superimposed (white triangles).**

© NOVELTIS, DTU, UCL, NPI 2021
This document is the property of NOVELTIS, no part of it shall be reproduced or transmitted without the express prior written authorisation of NOVELTIS

In order to better understand the reasons of this degradation in the regional simulations, we have run the hydrodynamic model in various configurations, for the three different bathymetry datasets (RTopo-2.0.4, BedMachine_Antarctica-2020-v2 and RTopo-1.0.5b), and varying the Hmin parameter of the model. This parameter gives the minimum value of water layer thickness considered by the model. For example, if Hmin=8 m, all the points where the depth is within [-8m;0m[ are set to -8 m. In very shallow water regions, it enables to smooth out local peaks in the bathymetry. In general, prescribing small Hmin values means that we trust the bathymetry in the shallow water regions.

Figure 24 shows the impact of the choice of bathymetry and Hmin value on the tidal simulations.

In the case of Rtopo-2.0.4 and Hmin=2 m, the tidal flow is strongly dissipated in the bays of the Rutford Ice Stream and Carlson Inlet, with very low amplitudes of M2, because the RTopo-2.0.4 bathymetry is extremely shallow (or indicates emerged land) in these areas. The M2 amplitude slightly increases when using Hmin= 8 m as the model artificially digs into the bathymetry down to 8 m. The same kind of process happens in the eastern part of the Korff Ice Rise.

The results are quite different with BedMachine_Antarctica-2020-v2, which clearly allows more tidal flow further into the Rutford and Carlson bays, even with Hmin=2 m. However, the vector differences at the two Rutford GPS stations are still very large, and the model locally overestimates the tidal amplitude by more than 1.50 m, which means it fails to adjust the dissipation due to the friction in the area.

The lower errors in the Rutford bay are obtained with the RTopo-1.0.5b bathymetry, with similar results to those obtained for the FES2014 hydrodynamic simulation.

Figure 25 shows the difference between the BedMachine_Antarctica-2020-v2 and the RTopo-1.0.5b bathymetry datasets in the area. Figure 26 shows the two bathymetry datasets, with different colour scales to focus either on the deeper regions or the shallower regions. The RTopo-1.0.5b bathymetry is clearly much deeper in the bays than the BedMachine dataset, with differences that can reach 300 meters. Deeper bays would also be more coherent with the strong basal melting that is observed in these regions. The RTopo-1.0.5b bathymetry dataset thus seems more coherent than the more recent bathymetry products in this region, in terms of depth. However, it can also be noticed that it is less coherent (locally shifted) with the recent GSHHS-2.3.7 coastline, and with the RTopo-2.0.4 grounding line position (Figure 22).

Regarding the grounding line itself, some clear differences with the coastline can be noted for the Evans Ice Stream, where one GPS station located close to the grounding line highlights large errors for all the tidal simulations (including FES2014). The RTopo-2.0.4 grounding line is also different from the GSHHS-2.3.7 coastline in part of the Rutford Ice Stream.

The model mesh grid limit is currently the GSHHS-2.3.7 coastline, but it should be the grounding line in such regions. Future work will consider the new grounding line product compiled in WP1.3, as explained in section 3.4. Further tidal simulation experiments will also be performed considering the new bathymetry dataset under the ice shelves produced within WP1.3.

© NOVELTIS, DTU, UCL, NPI 2021
This document is the property of NOVELTIS, no part of it shall be reproduced or transmitted without the express prior written authorisation of NOVELTIS

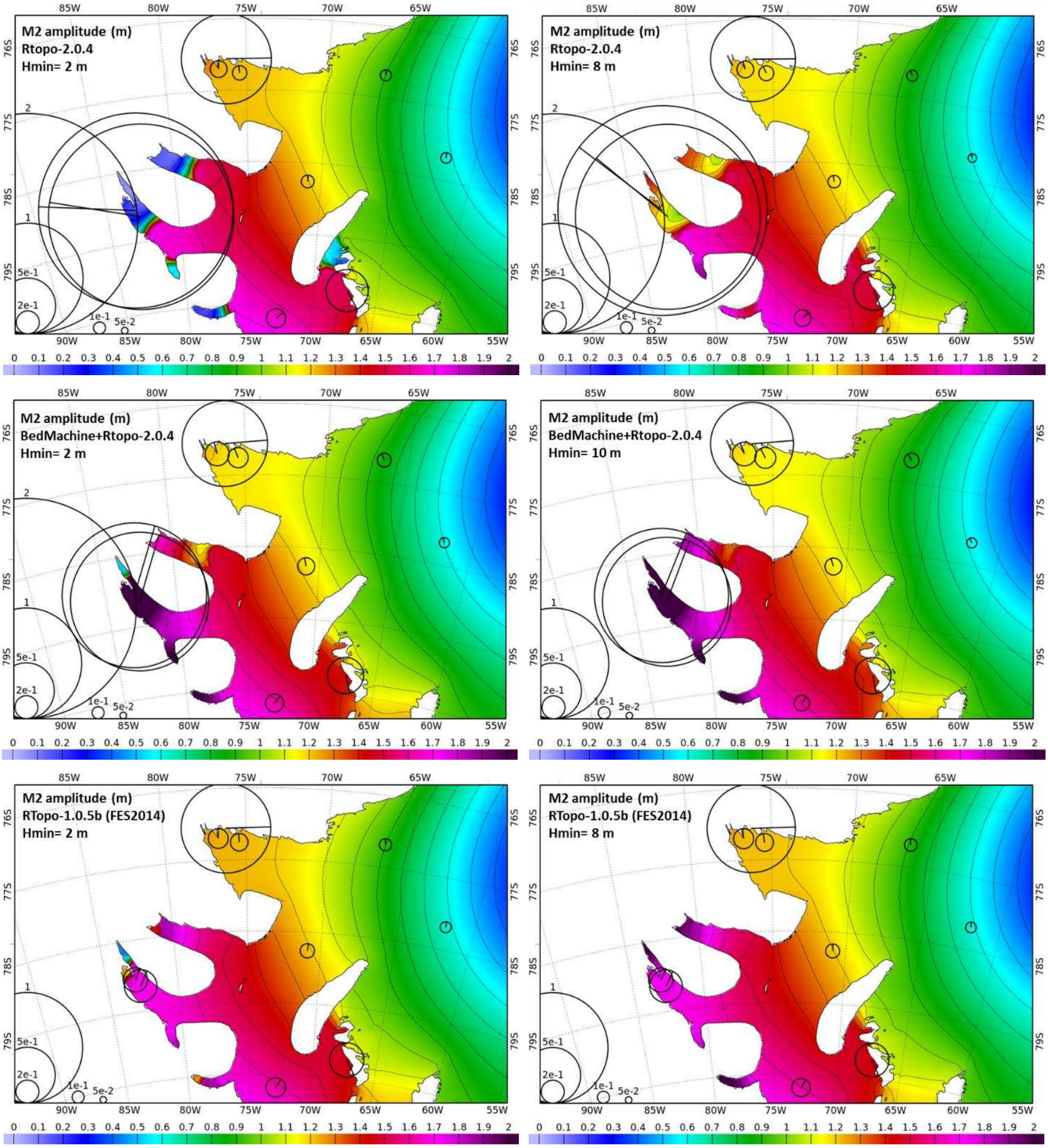


**Figure 24: Regional hydrodynamic simulations of the M2 tidal component (background colours show the amplitude in m) under the Filchner-Ronne ice shelf. Simulations based on the RTopo-2.0.4 bathymetry (upper plots, with Hmin=2 m on the left and Hmin=8 m on the right), the BedMachine_Antarctica-2020-v2 bathymetry (middle plots, with Hmin=2 m on the left and Hmin=10 m on the right), and the RTopo1.0.5b bathymetry (bottom plots, with Hmin=2 m on the left and Hmin=8 m on the right). The size of the black circles is proportional to the vector difference (in m) between the model and the tidal observations derived from in situ stations.**

© NOVELTIS, DTU, UCL, NPI 2021
This document is the property of NOVELTIS, no part of it shall be reproduced or transmitted without the express prior written authorisation of NOVELTIS

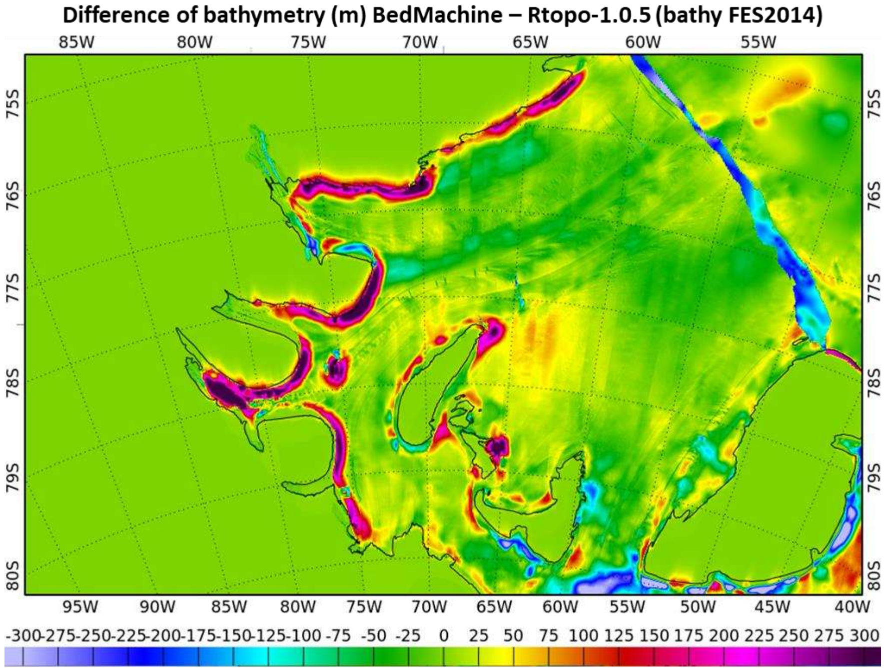


**Figure 25: Difference (in meters) between the BedMachine_Antarctica-2020-v2 and RTopo-1.0.5b bathymetry datasets under the Filchner-Ronne ice shelf (Weddell Sea).**

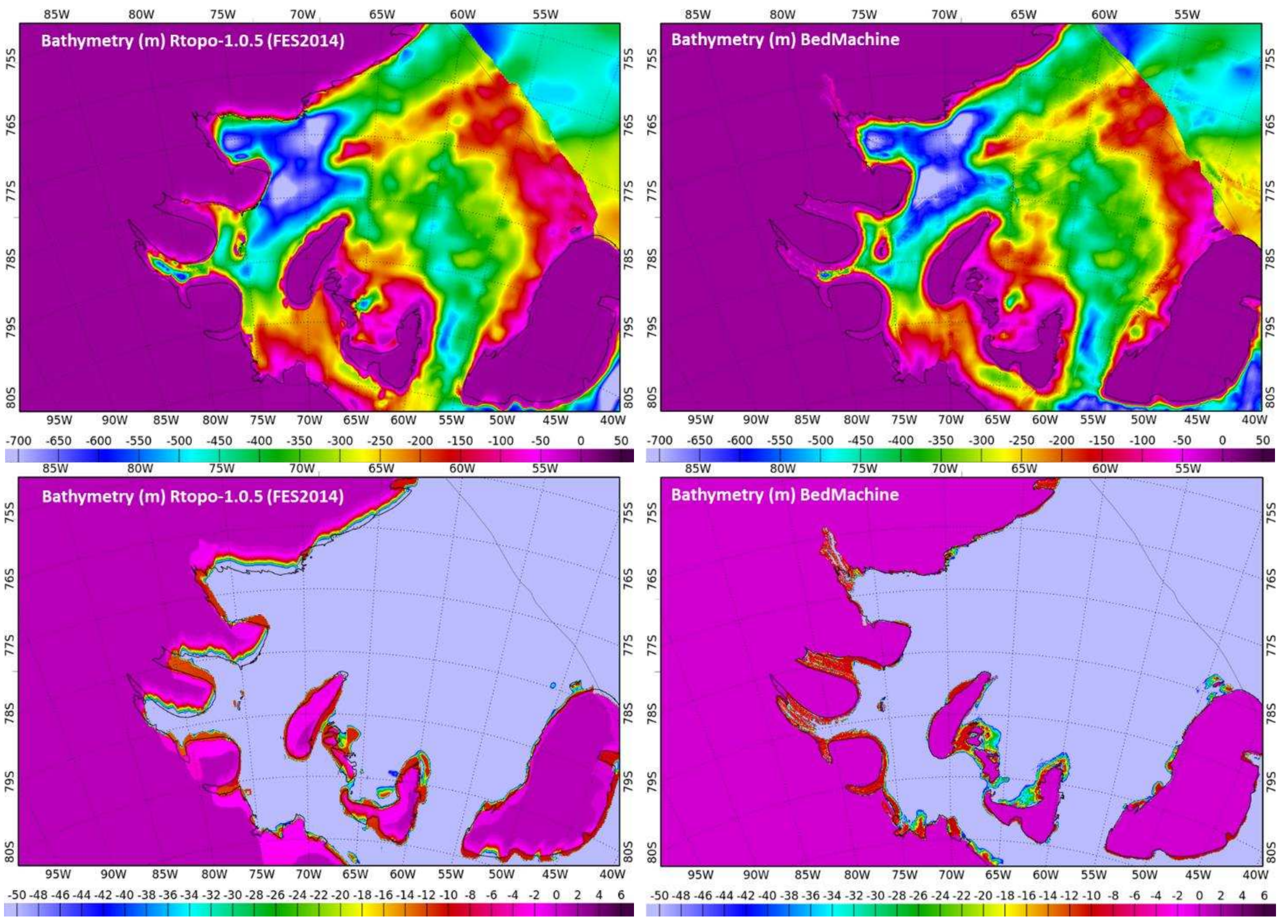


**Figure 26: RTopo-1.0.5b (left) and BedMachine_Antarctica-2020-v2 (right) bathymetry datasets under the Filchner-Ronne ice shelf. The upper plots focus on the deeper regions while the bottom plots focus on the shallow regions (different colour scales).**

© NOVELTIS, DTU, UCL, NPI 2021
This document is the property of NOVELTIS, no part of it shall be reproduced or transmitted without the express prior written authorisation of NOVELTIS

### 3.5.2. Case of the Amery ice shelf (East Antarctica)

The Amery ice shelf is the third ice shelf in terms of size in Antarctica. As observed in section 3.1.2, there is a much larger vector difference between the TS05 partially grounded Amery station (located close to the grounding line) and the tidal simulation based on BedMachine_Antarctica-2020-v2, than for the tidal simulation based on RTopo-2.0.4. Figure 27 shows a zoom in on these results under the Amery ice shelf. The results obtained with the regional tidal simulation based on the RTopo-1.0.5b bathymetry, as well as those of the FES2014 hydrodynamic solution (also based on RTopo-1.0.5b) are also presented. For each simulation, the amplitude (Amod) and the phase lag (Gmod) of the model at the TS05 Amery station are noted on the plot, as well as the in situ tidal constituents (Aobs and Gobs).

The BedMachine and RTopo-1.0.5b regional simulations, as well as the FES2014 global hydrodynamic simulation, give close results, with an overestimation of the tidal amplitude between 26 and 30 cm depending on the simulation. A shift of about 20 degrees is also noted on the phase lag. In the case of the RTopo-2.0.4 regional simulation, the tidal amplitude is underestimated by the model (2.9 cm instead of 6.4 cm). The phase lag is also strongly shifted. Finally, we can see that, close to the TS05 Amery station, the features of the M2 amplitude for this tidal simulation show a large decrease in tidal amplitude, compared to the other simulations.

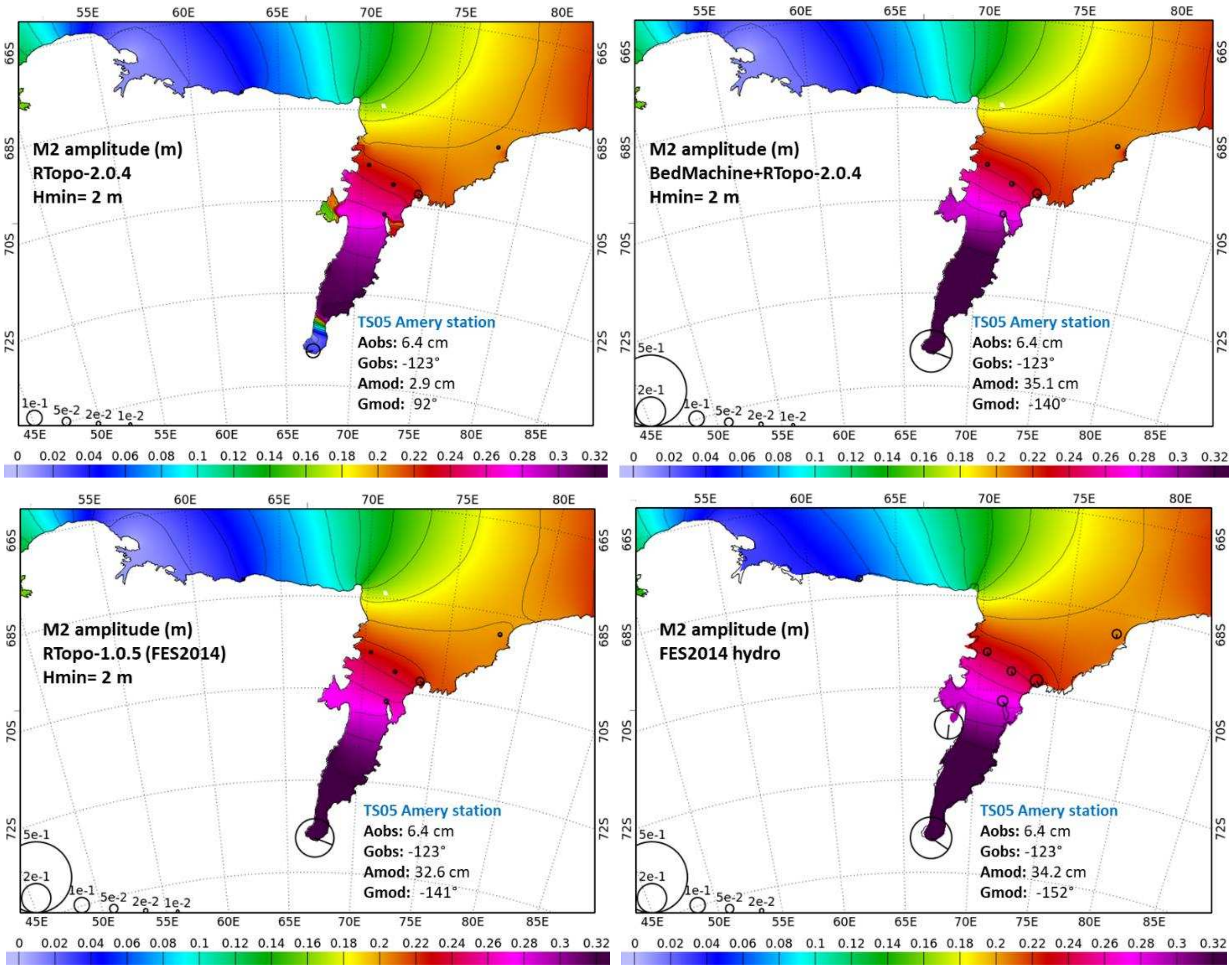


**Figure 27: Hydrodynamic simulations of the M2 tidal component (background colours show the amplitude in m) under the Amery ice shelf. Regional simulations based on the RTopo-2.0.4 bathymetry (upper plot, left), the BedMachine_Antarctica-2020-v2 bathymetry (upper plot, right), and the RTopo1.0.5b bathymetry (bottom plot, left). FES2014 hydrodynamic simulation based on RTopo-1.0.5b (bottom plot, right). The size of the black circles is proportional to the vector difference (in m) between the model and the tidal observations derived from in situ stations.**


© NOVELTIS, DTU, UCL, NPI 2021

This document is the property of NOVELTIS, no part of it shall be reproduced or transmitted without the express prior written authorisation of NOVELTIS

When looking at the bathymetry datasets in the region (Figure 28), it appears that RTopo-2.0.4 is much shallower than BedMachine_Antarctica-2020-v2 under the Amery ice shelf, especially in the most southern part. Like in the Filchner-Ronne ice shelf case, such shallow waters do not seem very coherent, and the BedMachine_Antarctica-2020-v2 and RTopo-1.0.5b bathymetry datasets are probably more relevant.

In this area, the dissipation in the tidal model due to the friction with the very shallow RTopo-2.0.4 bathymetry is much larger than for the other bathymetry datasets. It is highly probable that increasing the friction parameter in the model in this region for the simulation based on the BedMachine_Antarctica-2020-v2 should improve the consistency at the TS05 Amery station, and this will be tested in the near future.

It can also be noted that, in the case of the FES2014 hydrodynamic solution, an additional GPS station (Beaver Lake) provides some vector difference information with the model. Indeed, the coastline used in the case of the FES2014 model seems rather different from the GSHHS-2.3.7 coastline and RTopo-2.0.4 grounding line in this region, and further investigations will be performed in this area.

Finally, we can see that the vector differences with all the other in situ stations are clearly reduced with the regional tidal simulations, compared to the FES2014 global hydrodynamic simulation, which is a very encouraging result.

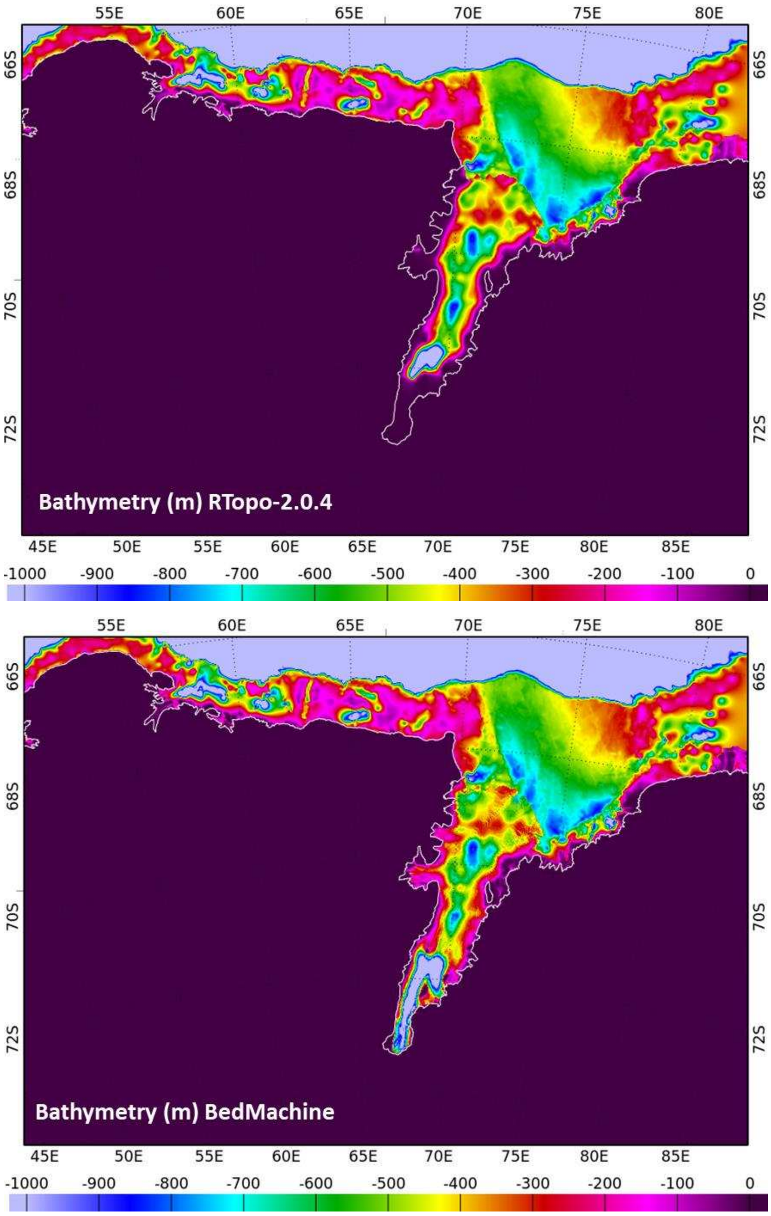


**Figure 28: RTopo-2.0.4 (upper plot) and BedMachine_Antarctica-2020-v2 (bottom plot) bathymetry datasets under the Amery ice shelf.**

© NOVELTIS, DTU, UCL, NPI 2021
This document is the property of NOVELTIS, no part of it shall be reproduced or transmitted without the express prior written authorisation of NOVELTIS

# 4. Conclusions

The work performed within the ALBATROSS project during the first period already provides very encouraging results.

A first version of the regional hydrodynamic tidal model configuration in the Southern Ocean has been implemented. Although still preliminary and not completely tuned, this regional configuration shows clear improvements compared to the FES2014 hydrodynamic solution in the region. Further developments are on-going as some improvements have been brought to the meshing tools and to the hydrodynamic TUGO model in the meantime.

Altimetry-derived tidal estimates have been computed by DTU using all the CryoSat-2 data processed with the SAMOSA+ retracker. This new dataset of altimetry-derived tidal constituents is very promising as it fills the gap between the 60°S-limited coverage of the TP-Jason-suite missions and the in-situ observations located along the Antarctica coast. In particular, this new dataset provides tidal data in the Weddell Sea, where other missions (ERS/Envisat/SARAL) cannot be used.

The available bathymetry datasets (at global and regional scales) have been inventoried and assessed in order to identify the most relevant dataset to be used as prior solution for the developments to be performed during the project. The combination of the BedMachine_Antarctica-2020-v2 and RTopo-2.0.4 bathymetry datasets appears to provide the best results in terms of tidal modelling. However, some further analyses under the Filchner-Ronne ice shelf, in the Weddell Sea, have shown that this bathymetry is too shallow in this region, and other datasets will be considered in the future work. In particular, the data compiled by NPI under the ice shelves, for the bathymetry and the grounding line, will be tested in the hydrodynamic tidal model. Further analyses in other regions will also be performed. This is an iterative process between tidal simulations and in-depth local investigations of the bathymetry.

The computation of the bathymetry combining the reference bathymetry (BedMachine+RTopo-2.0.4) and the new DTU21 gravity field is on-going. Several of the processing steps, which are time-consuming computations, have been achieved and already show some potential improvements thanks to the CryoSat-2 data in the Southern Ocean.

The computation of the sea ice roughness characteristics based on MISR and OIB data is also on-going at UCL. The algorithms have been fine-tuned, first in the Arctic Ocean and then to produce a first month of data in the Southern Ocean. Huge quantities of data are being processed, which demands a lot of computation time, but the first results are quite encouraging.

© NOVELTIS, DTU, UCL, NPI 2021
This document is the property of NOVELTIS, no part of it shall be reproduced or transmitted without the express prior written authorisation of NOVELTIS